Supporting Information

Distinguishing Between Aquo and Hydroxo Coordination in Molecular Copper Complexes by ^{1}H and ^{17}O ENDOR Spectroscopy

Julia Haak,[a,b] George E. Cutsail III[a,b,*]

[a] Max Planck Institute for Chemical Energy Conversion, Stiftstrasse 34-36, D-45470 Mülheim an der Ruhr, Germany

[b] Institute of Inorganic Chemistry, University of Duisburg-Essen, Universitätsstrasse 5-7, D-45141, Essen, Germany

email: george.cutsail@cec.mpg.de

Contents

Spectrometer Conditions 4

Table S1. CW X-band EPR (room temperature). 4

Table S2. CW X-band EPR (cryogenic temperatures). 4

Table S3. Pulsed Q-band EPR. 5

Table S4. Q-band ^{1}H ENDOR. 5

Table S5. Q-band ^{14}N/^{17}O ENDOR. 5

Table S6. Pulsed W-band EPR. 6

Table S7. W-band ^{14}N/^{17}O EDNMR. 6

Influence of glassing agent 7

Figure S1. CW X-band EPR without glassing agent. 7

UV-Vis Spectroscopy 8

Figure S2. UV-Vis pH titration. 8

Cyclic Voltammograms 9

Figure S3. Cyclic Voltammograms at several pH values. 9

Multifrequency EPR and ^{14}N ENDOR Characterization 10

Figure S4. X-, Q- and W-band EPR and ^{14}N ENDOR spectra of **Cu-I**. 10

Figure S5. X-, Q- and W-band EPR and ^{14}N ENDOR spectra of **Cu-III**. 11

Figure S6. X-, Q- and W-band EPR spectra of **Cu-IV**. 12

Figure S7. Comparison of the X- and Q-band EPR spectra of **Cu-I** and **Cu-V**. 13

Figure S8. X- and Q-band EPR and ^{14}N ENDOR spectra of of **Cu-V**. 14

Figure S9. X- and Q-band EPR and ^{14}N ENDOR spectra of **Cu-VI**. 15

Table S8. EPR and ^{14}N ENDOR simulation parameters I 16

Table S9. EPR and ^{14}N ENDOR simulation parameters II 17

Room Temperature EPR 18

Figure S10. CW X-band EPR titration with simulations.. 18

Table S10. Room temperature X-band EPR simulation parameters.. 19

Table S11. Relative amounts of copper complexes observed by X-band EPR 20

Figure S11. Room temperature EPR of **Cu-I**: Determining relative signs. 21

^{1}H ENDOR 22

Figure S12. ^{1}H/^{2}H ENDOR subtractions of **Cu-I**.. 22

Figure S13. ^{1}H/^{2}H ENDOR subtractions of **Cu-III**.. 22

Figure S14. ^{1}H ENDOR spectra of **Cu-IV**. 23

Figure S15. ^{1}H/^{2}H ENDOR subtractions of **Cu-V**. 23

Figure S16. ^{1}H/^{2}H ENDOR subtractions of **Cu-VI**. 24

Figure S17. Exchangeable proton resonances of **Cu-I** with simulations. 24

Figure S18. Exchangeable proton resonances of **Cu-III** with simulations........................25
Figure S19. Exchangeable proton resonances of **Cu-IV** with simulations........................26
Figure S20. Exchangeable proton resonances of **Cu-V** with simulations. 27
Figure S21. Exchangeable proton resonances of **Cu-VI** with simulations........................27
Table S12. ^{1}H ENDOR simulation parameters. 28
Figure S22. Comparison of ^{1}H ENDOR spectra of **Cu-I**, **Cu-III**, **Cu-V** and **Cu-VI**. 28
Table S13. ^{1}H hyperfine couplings found in literature...29
Table S14. ^{17}O hyperfine couplings found in literature. 30
^{14}N ENDOR 31
Figure S23. ^{14}N/^{17}O ENDOR subtractions of **Cu-I**.. 31
Figure S24. ^{14}N/^{17}O ENDOR subtractions of **Cu-III**. 32
Figure S25. ^{14}N/^{17}O ENDOR subtractions of **Cu-IV**. 32
Figure S26. ^{14}N/^{17}O ENDOR subtractions of **Cu-V**. 33
Figure S27. ^{14}N/^{17}O ENDOR subtractions of **Cu-VI**. 33
Figure S28. Comparison of ^{14}N ENDOR spectra of **Cu-I**, **Cu-III**, **Cu-V** and **Cu-VI**. 34
Figure S29. ^{17}O ENDOR resonances of **Cu-III** with simulations. 35
Figure S30. ^{17}O ENDOR resonances of **Cu-IV** with simulations. 35
Figure S31. ^{17}O ENDOR resonances of **Cu-V** with simulations. 36
Table S15. ^{14}N/ ^{17}O ENDOR simulation parameters. 36
EDNMR 37
Figure S32. W-band EDNMR spectra of **^{17}O-Cu-I**: raw data and baseline subtraction.....37
Figure S33. W-band EDNMR spectra of **Cu-I**: raw data and baseline subtraction............38
Figure S34. W-band EDNMR spectra of **^{17}O-Cu-III**: raw data and baseline subtraction. 39
Figure S35. W-band EDNMR spectra of **Cu-III**: raw data and baseline subtraction.........40
Figure S36. W-band EDNMR spectra of **^{17}O-Cu-IV**: raw data and baseline subtraction..41
Figure S37. ^{14}N/^{17}O EDNMR subtractions of **Cu-I**...42
Figure S38. ^{14}N/^{17}O EDNMR subtractions of **Cu-III**..42
Figure S39. ^{17}O EDNMR resonances of **Cu-III** with simulations. 43
Figure S40. ^{17}O EDNMR resonances of **Cu-IV** with simulations...................................44
Computational Studies 45
Table S16. Calculated EPR parameters of **DFT-I**, **DFT-II**, **DFT-III** and **DFT-IV**. 45
Coordinates of DFT Optimized Structures 46
Figure S41. Cu-IV after O-Cu-O angle constraints with t / a_{iso} angle dependence. 57
Table S17. Calculated EPR parameters of **Cu-IV** after O-Cu-O angle constraints. 57
References..58

Spectrometer Conditions

Table S1. Spectrometer Conditions for CW X-band EPR measurements of copper bipyridine solutions collected at room temperature.

Microwave frequency [GHz]	9.43
Number of points	~60,000
Shots per point	1
Number of scans	1
Modulation amplitude [G]	8 (pH 6.1 – 12.7) 6 (pH 13.7)
Modulation amplitude [kHz]	100
Sweep time [s]	240 (pH 6.1 – 12.7) 360 (pH 13.7)
Effective time constant [s]	0.05

Table S2. Spectrometer Conditions for CW X-band EPR measurements of copper bipyridine solutions collected at cryogenic temperatures.

	Cu-I	**Cu-III**	**Cu-IV**	**Cu-V**	**Cu-VI**
Microwave frequency [GHz]	9.46	9.46	9.45	9.47	9.45
Number of points	~60,000	~60,000	~30,000	~30,000	~60,000
Shots per point	1	1	1	1	1
Number of scans	3	3	1	1	3
Modulation amplitude [G]	6	6	6	6	6
Modulation amplitude [kHz]	100	100	100	100	100
Sweep time [s]	240	240	180	120	360
Effective time constant [s]	0.05	0.05	0.05	0.05	0.05
Temperature [K]	77	77	77	100	77

Table S3. Spectrometer Conditions for pulsed Q-band EPR measurements of copper bipyridine solutions.

	Cu-I	**Cu-III**	**Cu-IV**	**Cu-V**	**Cu-VI**
Microwave frequency [GHz]	33.99	34.00	33.97	34.00	33.94
Number of points	4,096	4,096	4,096	4,096	4,096
Shots per point	100	20	10	5	100
Number of scans	1	1	1	1	1
$\pi/2$ [ns]	40	40	40	20	40
τ [ns]	400	400	400	400	450
Shot repetition rate [us]	1,000	5,000	2,000	2,000	1,750
Temperature [K]	12	10	16	28	12

Table S4. Spectrometer Conditions for Q-band ^{1}H ENDOR measurements of copper bipyridine solutions.

	Cu-I	**Cu-III**	**Cu-IV**	**Cu-V**	**Cu-VI**
$\pi/2$ [ns]	40	40	40	40	40
τ [ns]	400	400	400	400	420
T_{RF} [us]	10	10	10	20	10
t_{wait} [us]	2	2	2	2	2
Shot repetition rate [us]	1,500	1,500 (H_2O) 3,000 (D_2O)	2,000	7,000	3,000
Microwave frequency [GHz]	34.01	34.00 (H_2O) 33.99 (D_2O)	33.97	33.97 (H_2O) 34.00 (D_2O)	33.96 or 34.00 (H_2O) 34.00 (D_2O)
Temperature [K]	12	8.5 (H_2O) 12 (D_2O)	16	12	8.5
Number of points	1,024	1,024	1,000	1,024	1,000 (H_2O) 800 – 1,000 (D_2O)
Shots per point	10 (H_2O) 3-10 (D_2O)	3 (H_2O) 10 (D_2O)	1	1	3
Number of scans	44-167 (H_2O) 87-276 (D_2O)	19-47 (H_2O) 14-130 (D_2O)	19-125 (H_2O) 47-91 (D_2O)	10 – 82 (H_2O) 20 – 142 (D_2O)	26 – 112 (H_2O) 79 – 133 (D_2O)

Table S5. Spectrometer Conditions for Q-band ^{14}N/^{17}O ENDOR measurements of copper bipyridine solutions.

	Cu-I	**Cu-III**	**Cu-IV**	**Cu-V**	**Cu-VI**
$\pi/2$ [ns]	40 (^{14}N) 24 (^{17}O)	16	16	40	40
τ [ns]	400	400	420	400	400
T_{RF} [us]	30	30	15	20	10
t_{wait} [us]	2	2	1	2	2
Shot repetition rate [us]	5,000	5,000	3,000 (^{14}N) 5,000 (^{17}O)	8,000 (^{14}N) 7,000 (^{17}O)	4,000
Microwave frequency [GHz]	33.98 (^{14}N) 33.96 (^{17}O)	33.95	33.98	34.00	34.00

Temperature [K]	8.5	10	15	12	8
Number of points	800 – 1200	1,200	1,000	1,000	1,000
Shots per point	1	1	1	1	3
Number of scans	155-838 (^{14}N) 159-570 (^{17}O)	116-589 (^{14}N) 246-611 (^{17}O)	106 (^{14}N) 40-95 (^{17}O)	63-176 (^{14}N) 25-174 (^{17}O)	104-297 (^{14}N) 123-161 (^{17}O)

Table S6. Spectrometer Conditions for pulsed W-band EPR measurements of copper bipyridine solutions.

	Cu-I	**Cu-III**	**Cu-IV**
Microwave frequency [GHz]	94.03	94.02	94.05
Number of points	5,000	5,000	5,000
Shots per point	150	60	50
Number of scans	1	1	1
$\pi/2$ [ns]	20	20	20
τ [ns]	600	400	1,200
Shot repetition rate [us]	2,000	2,000	3,000
Temperature [K]	9	10	10

Table S7. Spectrometer Conditions for W-band $^{14}N/^{17}O$ EDNMR measurements of copper bipyridine solutions.

	Cu-I	**Cu-III**	**Cu-IV**
$\pi/2$ [ns]	100	100	200
τ [ns]	1000	1000	1,500
T_{HTA} [us]	30	60	30
t_{wait} [us]	6	6	2
Shot repetition rate [us]	1,000	7,500 (^{14}N) 15,000 (^{17}O)	2,500
Microwave frequency [GHz]	94.03 (^{14}N) 94.01 (^{17}O)	93.99 (^{14}N) 93.94 (^{17}O)	94.05
Temperature [K]	9	6	10
Number of points	1,000	2,000	6,000
Shots per point	50	50	20
Number of scans	126-600 (^{14}N) 54-512 (^{17}O)	8-35 (^{14}N) 2-27 (^{17}O)	1-76

Influence of glassing agent

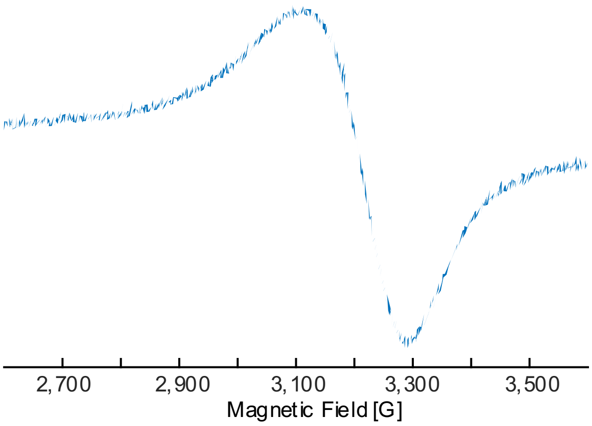

Figure S1. CW X-band (9.45 GHz, 77 K) spectrum of copper bipyridine (1:1 ratio) in water without added NaOAc (or glycerol) showing a broad EPR response.

UV-Vis Spectroscopy

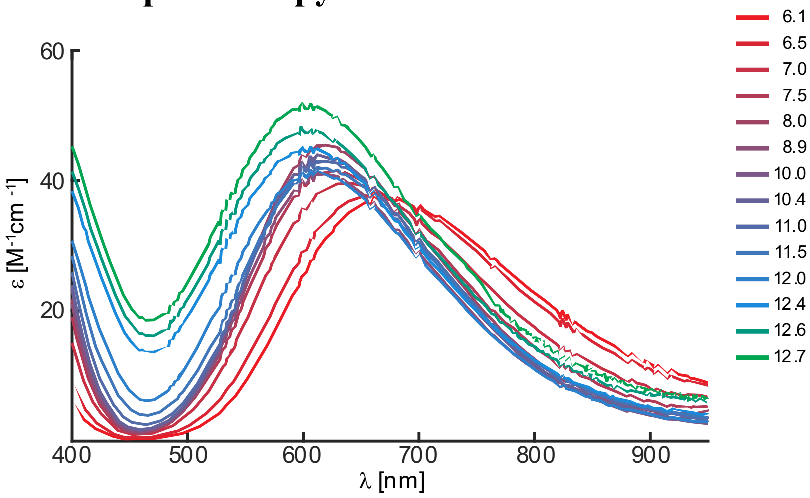

Figure S2. Absorption spectra of copper bipyridine solutions at several pH values.

Cyclic Voltammograms

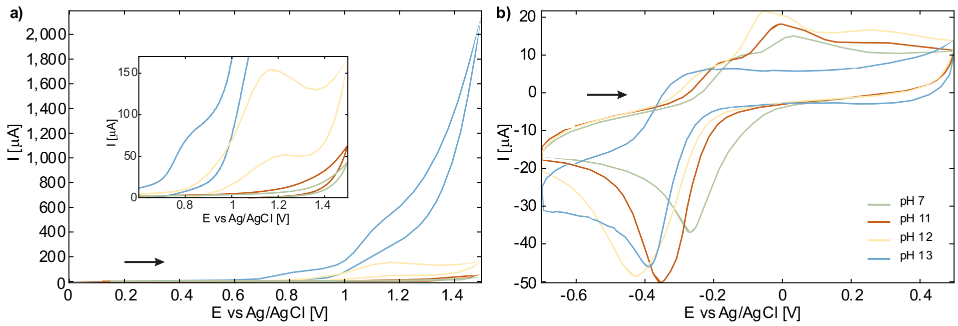

Figure S3. Cyclic Voltammograms of copper bipyridine solutions (1 mM, 0.1 M NaOAc) at several pH values, scanned with a scan rate of 0.1 V/s, showing the Cu(II)/Cu(III) (**a**) and the Cu(I)/Cu(II) (**b**) couple. The arrows indicate the sweep direction.

Multifrequency EPR and ^{14}N ENDOR Characterization

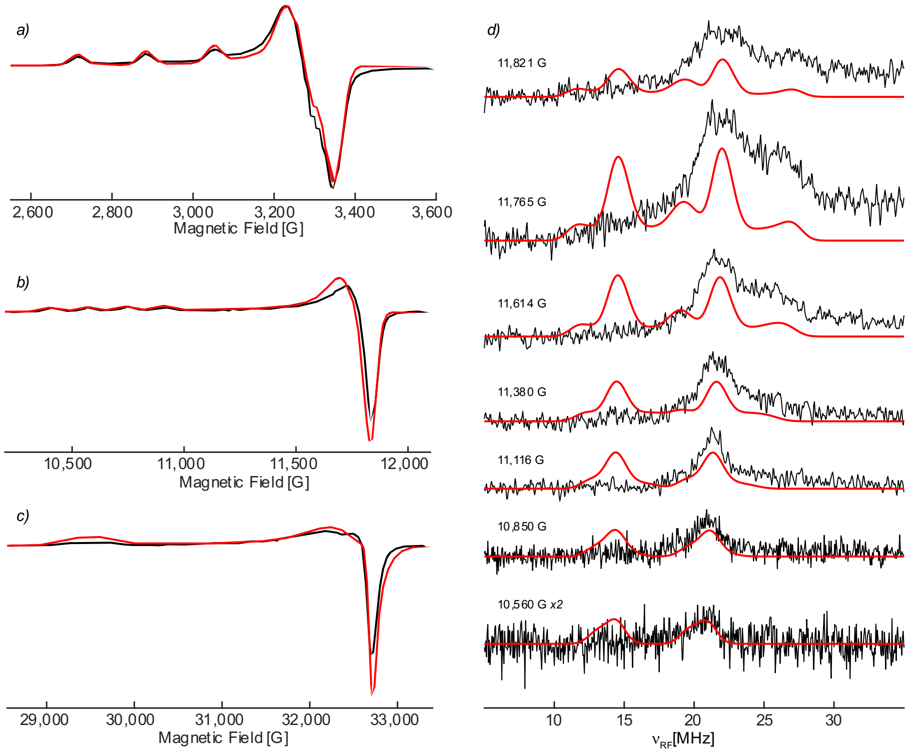

Figure S4. CW X-band (**a**) and numerical derivatives of the pulsed Q- (**b**) and W-band (**c**) EPR and ^{14}N Davies ENDOR (**d**) spectra of **Cu-I** in black with simulations in red. An ENDOR linewidth of 1.5 mT (full width at half height) was applied. Other simulation parameters are reported in **Table S8**. Spectrometer Conditions are listed in the Experimental Section. The relative intensities of the ENDOR features are distorted due to the lower frequency limit of the employed resonator (cut off approximately below 18 MHz; see main text).

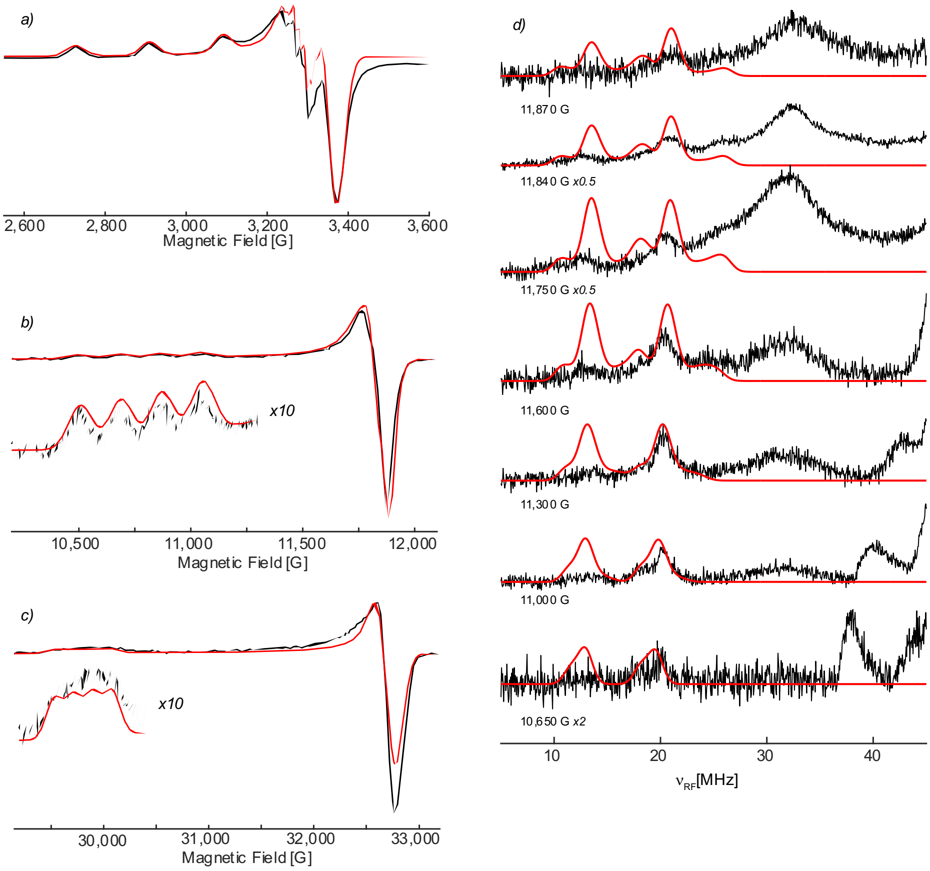

Figure S5. CW X-band (**a**) and numerical derivatives of the pulsed Q- (**b**) and W-band (**c**) EPR and ^{14}N Davies ENDOR (**d**) spectra of **Cu-III** in black with simulations in red. An ENDOR linewidth of 1.5 mT (full width at half height) was applied. Other simulation parameters are reported in **Table S8**. Spectrometer Conditions are listed in the Experimental Section. The relative intensities of the ENDOR features are distorted due to the lower frequency limit of the employed resonator (cut off approximately below 18 MHz; see main text).

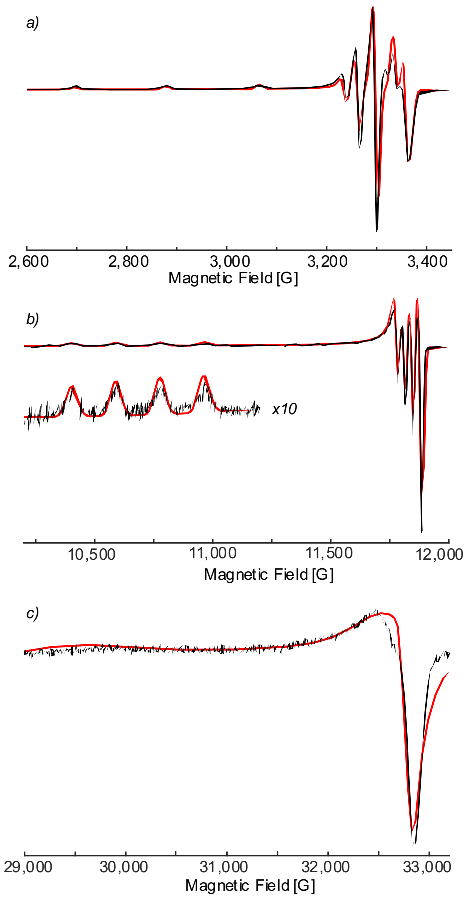

Figure S6. CW X-band (**a**) and numerical derivatives of the pulsed Q- (**b**) and W-band (**c**) EPR spectra of **Cu-IV** in black with simulations in red. Simulation parameters are reported in **Table S8**. Spectrometer Conditions are listed in the Experimental Section.

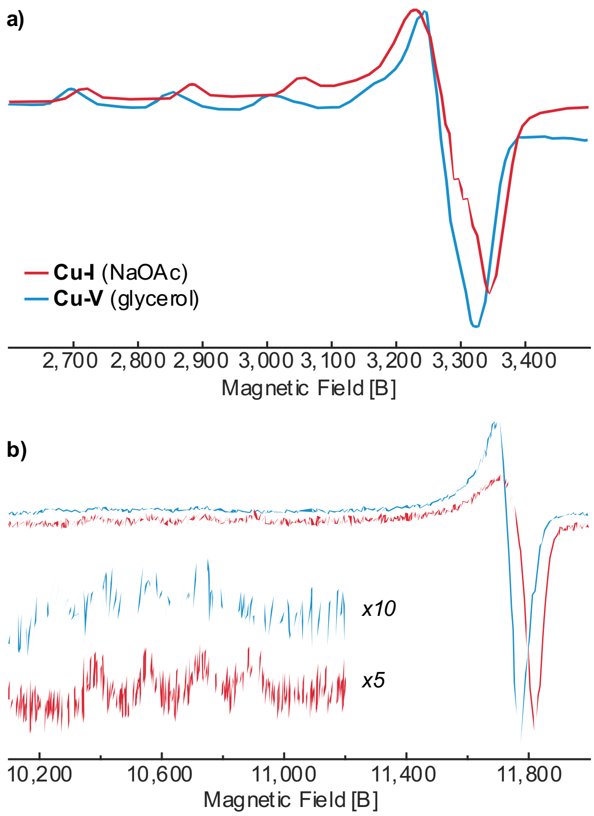

Figure S7. CW X-band (**a**) and numerical derivatives of the pulsed Q-band (**b**) EPR spectra of **Cu-I** and **Cu-V**. Spectrometer Conditions are listed in the Experimental Section.

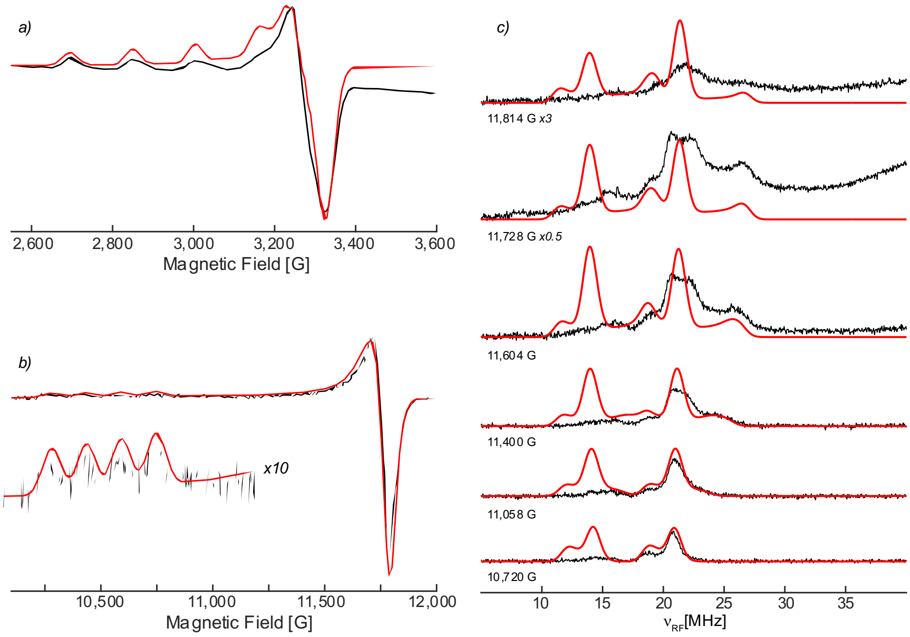

Figure S8. CW X-band (**a**) and numerical derivative of the pulsed Q-band (**b**) EPR and Q-band ENDOR (**c**) spectra of of **Cu-V** in black with simulations in red. An ENDOR linewidth of 1.2 mT (full width at half height) was applied. Other simulation parameters are reported in **Table S9**. Spectrometer Conditions are listed in the Experimental Section. The relative intensities of the ENDOR features are distorted due to the lower frequency limit of the employed resonator (cut off approximately below 18 MHz; see main text).

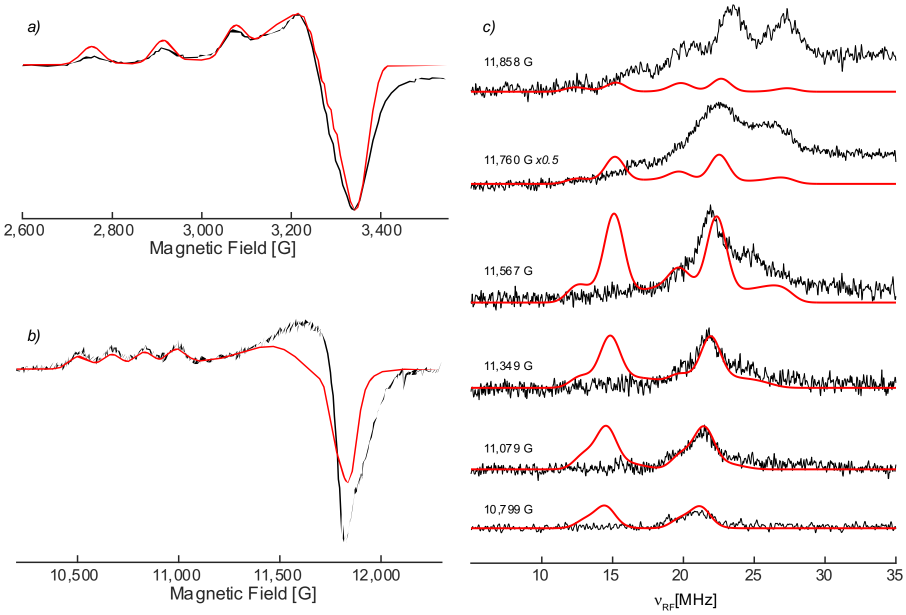

Figure S9. CW X-band (**a**) and numerical derivative of the pulsed Q-band (**b**) EPR and Q-band ENDOR (**c**) spectra of **Cu-VI** in black with simulations in red. An ENDOR linewidth of 1.5 mT (full width at half height) was applied. Other simulation parameters are reported in **Table S9**. Spectrometer Conditions are listed in the Experimental Section. The relative intensities of the ENDOR features are distorted due to the lower frequency limit of the employed resonator (cut off approximately below 18 MHz; see main text).

Table S8. Simulation parameters of **Cu-I, Cu-III** and **Cu-IV** obtained from X-, Q- and W-band EPR and Q-band ENDOR simulation (**Figures S4-S6**).

	Cu-I	**Cu-III**	**Cu-IV**
$\mathbf{g} = [g_1, g_2, g_3]$	[2.278±0.001, 2.068±0.003, 2.055±0.001]	[2.254±0.001, 2.055±0.001, 2.050±0.002]	[2.272±0.0005, 2.053±0.0005, 2.050±0.0005]
g_{iso} [a)]	2.134	2.120	2.125
$\mathbf{A}(^{63}Cu) = [A_1, A_2, A_3]$ in MHz [b)]	[525±7, 43±10, 36±10]	[560±5, 64±10, 62±10]	[582±4, 90±5, 92±5]
$\mathbf{A}(^{14}N) = [A_1, A_2, A_3]$ in MHz	[34, 34, 42] [34, 42, 34]	[31, 32, 40] [31, 40, 32]	[-]
$\mathbf{P}(^{14}N) = [P_1, P_2, P_3]$ in MHz	[0.5, 1.4 -1.9] [0.5, -1.9, 1.4]	[0.5, 1.4 -1.9] [0.5, -1.9, 1.4]	[-]
gStrain	X: [0.02 0.04 0] Q: [0.02 0.02 0] W: [0.03 0.04 0]	S: [0.01 0 0.02] X: [0.03 0 0.03] Q: [0.025 0.02 0] W: [0 0 0]	X: [0 0 0] Q: [0.01 0 0] W: [0.08 0.04 0]
Linewidth in mT (gaussian peak-to-peak)	X: 1 Q: 1.5 W: 5	S: 1 X: 0.8 Q: 0.9 W: 15	X: 1 Q: 1.8 W: 5

a) The isotropic components of the **g**- and **A**-tensors were calculated as follows: $a_{iso} = \frac{A_1+A_2+A_3}{3}$ and $g_{iso} = \frac{g_1+g_2+g_3}{3}$.

b) Copper hyperfine couplings are reported for the ^{63}Cu isotope. Simulations consider also the ^{65}Cu isotope with hyperfine couplings that are scaled by the gyromagnetic ratio of both nuclei: $\gamma = \frac{|g_n(^{63}Cu)|}{|g_n(^{65}Cu)|} = \frac{|A(^{63}Cu)|}{|A(^{65}Cu)|}$.

Table S9. Simulation parameters of **Cu-V** and **Cu-VI** obtained from X- and Q-band EPR and Q-band ENDOR simulation together with the estimated uncertainties for some parameters (**Figure S8** and **S9**).

	Cu-V	**Cu-VI**
g = [g_1, g_2, g_3]	[2.310±0.002, 2.068±0.003, 2.064±0.002]	[2.255±0.002, 2.090±0.01, 2.055±0.005]
g_{iso} [a)]	2.147	2.133
A(^{63}Cu) = [A_1, A_2, A_3] in MHz [b)]	[490±8, 43±15, 36±15]	[495±7, 75±20, 85±20]
A(^{14}N) = [A_1, A_2, A_3] in MHz	[33, 33, 41] [33, 41, 33]	[34, 35, 43] [34, 35, 43] [34, 43, 35] [34, 43, 35]
P(^{14}N) = [P_1, P_2, P_3] in MHz	[0.8, 1.1 -1.9] [0.8, -1.9, 1.1]	[0.5, 1.2, -1.7] [0.5, 1.2, -1.7] [0.5, -1.7, 1.2] [0.5, -1.7, 1.2]
gStrain	X: [0.02 0.04 0] Q: [0.02 0.02 0]	X: [0.02 0.04 0] Q: [0.02 0.06 0]
Linewidth in mT (gaussian peak-to-peak)	X: 1 Q: 1.5	X: 1 Q: 1.5

a) The isotropic components of the **g**- and **A**-tensors were calculated as follows: $a_{iso} = \frac{A_1+A_2+A_3}{3}$ and $g_{iso} = \frac{g_1+g_2+g_3}{3}$.

b) Copper hyperfine couplings are reported for the ^{63}Cu isotope. Simulations consider also the ^{65}Cu isotope with hyperfine couplings that are scaled by the gyromagnetic ratio of both nuclei: $\gamma = \frac{|g_n(^{63}Cu)|}{|g_n(^{65}Cu)|} = \frac{|A(^{63}Cu)|}{|A(^{65}Cu)|}$.

Room Temperature EPR

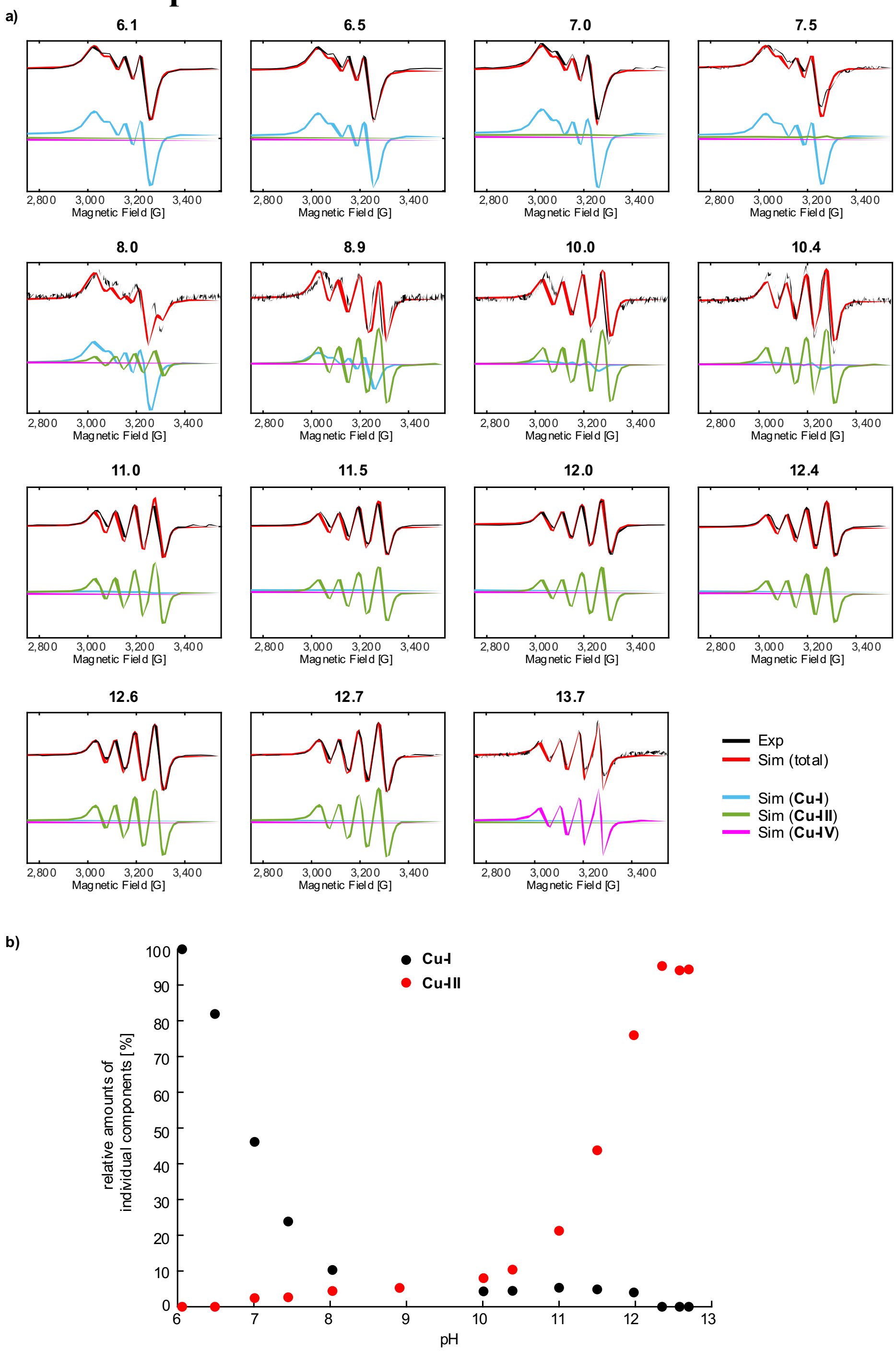

Figure S10. (**a**) CW X-band (9.43 GHz) EPR spectra of copper bipyridine solutions at several pH values in black with respective simulations in color. The simulations of the individual components are shown in blue (**Cu-I**), green (**Cu-III**) and magenta (**Cu-IV**), and the summed simulation in red. Simulation parameters are listed in **Table S10**. The relative amounts of the individual species are listed in **Table S11**, which is visualized in (**b**) for **Cu-I** and **Cu-III**. Spectrometer conditions are described in the Experimental Section.

Table S10. Simulation parameters of room temperature X-band EPR spectra (**Figure S10**). The relative weightings are reported in **Table S11**.

Simulation parameters of room temperature spectra			
	Cu-I	**Cu-III**	**Cu-IV**
$\mathbf{g} = [g_1, g_2, g_3]$	[2.284, 2.074, 2.061]	[2.254, 2.055, 2.050]	[2.277, 2.058, 2.055]
g_{iso} [a)]	2.140	2.120	2.130
$\mathbf{A}(^{63}Cu) = [A_1, A_2, A_3]$ in MHz [b)]	[-525, +43, -36]	[-560, -64, -62]	[-582, -40, -40]
$a_{iso}(^{63}Cu)$ in MHz [a)]	-173	-229	-221
Linewidth in mT (gaussian and lorentzian peak-to-peak)[c)]	[4.3, 1.1]	[2.8, 1.2]	[1.0, 2.0]
Rotational correlation time in s (isotropic) [c)]	(3.5±0.3)*1e-11	(2.5±0.4)*1e-11	(2±0.6)*1e-11

a) The isotropic components of the **g**- and **A**-tensors were calculated as follows: $a_{iso} = \frac{A_1+A_2+A_3}{3}$ and $g_{iso} = \frac{g_1+g_2+g_3}{3}$.

b) Copper hyperfine couplings are reported for the ^{63}Cu isotope. Simulations consider also the ^{65}Cu isotope with hyperfine couplings that are scaled by the gyromagnetic ratio of both nuclei: $\gamma = \frac{|g_n(^{63}Cu)|}{|g_n(^{65}Cu)|} = \frac{|A(^{63}Cu)|}{|A(^{65}Cu)|}$.

c) To simulate the motially averaged spectra of the copper bipyridine solutions, the spin Hamiltonian parameters (i. e. g-values and the Cu hyperfine) were chosen in conjunction with the ones for the powder pattern simulations and only minimally adjusted. Subsequently, the rotational correlation time was chosen to reproduce the relative intensities of the individual features of the oberserved quartets. Lastly, the gaussian and lorentzian linewidths were adjusted to represent the overall lineshape of the individual features.

Table S11. Relative amounts of the individual copper complexes in copper bipyridine solutions at several pH values, obtained by X-band EPR simulations (**Figure S10**).

pH	**Cu-I**	**Cu-III**	**Cu-IV**
6.1	100 %	0 %	0 %
6.5	100 %	0 %	0 %
7.0	95 %	5 %	0 %
7.5	90 %	10 %	0 %
8.0	70 %	30 %	0 %
8.9	50 %	50 %	0 %
10.0	35 %	65 %	0 %
10.4	30 %	70 %	0 %
11.0	20 %	80 %	0 %
11.5	10 %	90 %	0 %
12.0	5 %	95 %	0 %
12.4	0 %	100 %	0 %
12.6	0 %	100 %	0 %
12.7	0 %	100 %	0 %
13.7 [a)]	0 %	0 %	100 %

[a)] The EPR spectrum at pH 13.7 was not obtained through the pH titration, but added individually by using a stronger base.

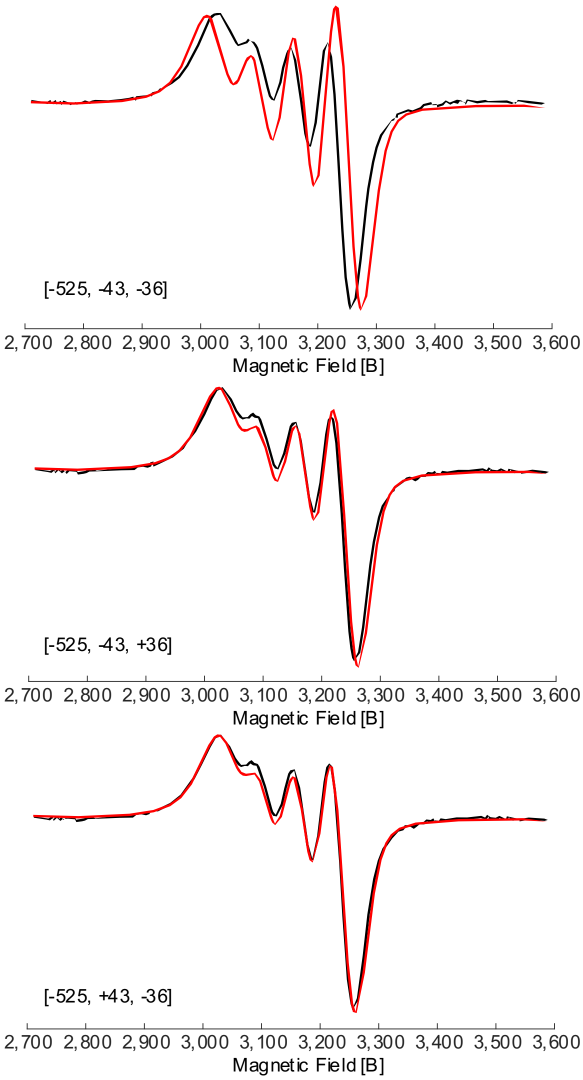

Figure S11. Room temperature X-band EPR spectrum of **Cu-I** in black with simulation in red, using Cu hyperfine tensors of **A** = [-525, -43, -36] MHz (top), **A** = [-525, -43, +36] MHz (middle) and **A** = [-525, +43, -36] MHz (bottom), showing that one of the $A_{\perp}$(Cu) values has to be positive, with a slight favouring of the third case.

[1]H ENDOR

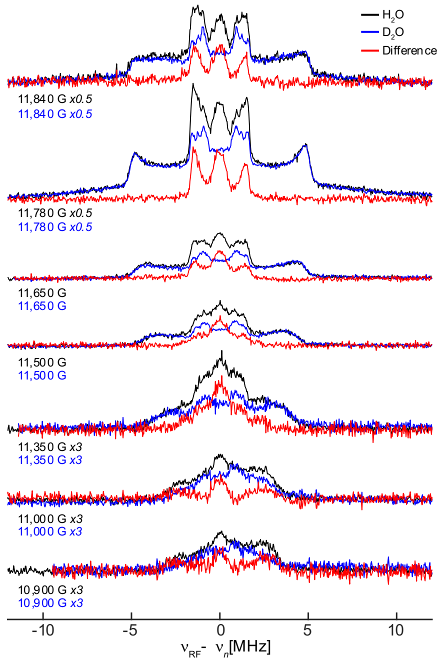

Figure S12. Q-band [1]H Davies ENDOR spectra of **Cu-I** for samples prepared in H_2O (black) and D_2O (blue). The subtraction of the two is depicted is shown in red. Spectrometer Conditions are listed in the Experimental Section and **Table S4**.

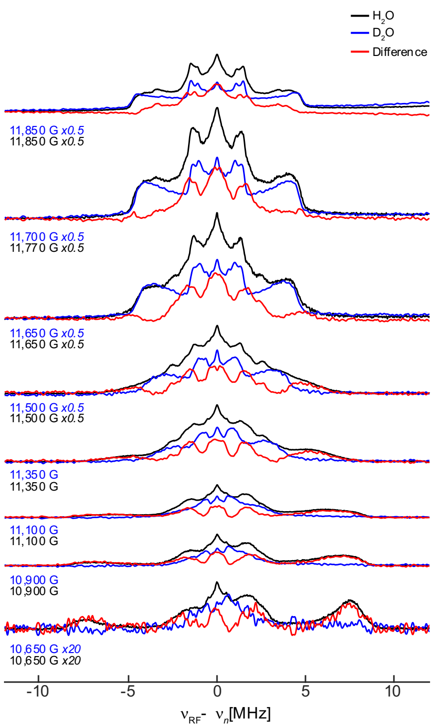

Figure S13. Q-band [1]H Davies ENDOR spectra of **Cu-III** for samples prepared in H_2O (black) and D_2O (blue). The subtraction of the two is depicted is shown in red. Spectrometer Conditions are listed in the Experimental Section and **Table S4**.

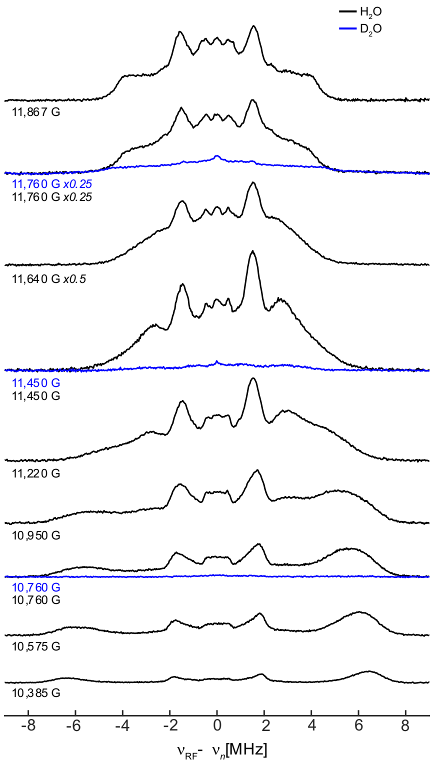

Figure S14. Q-band [1]H Davies ENDOR spectra of **Cu-IV** for samples prepared in H_2O (black) and D_2O (blue), normalized for the number of scans and the VideoGain. The latter one exhibits barely any [1]H resonances, confirming that all protons of **Cu-IV** are exchangeable due to the loss of the bipyridine ligand. Spectrometer Conditions are listed in the Experimental Section and **Table S4**.

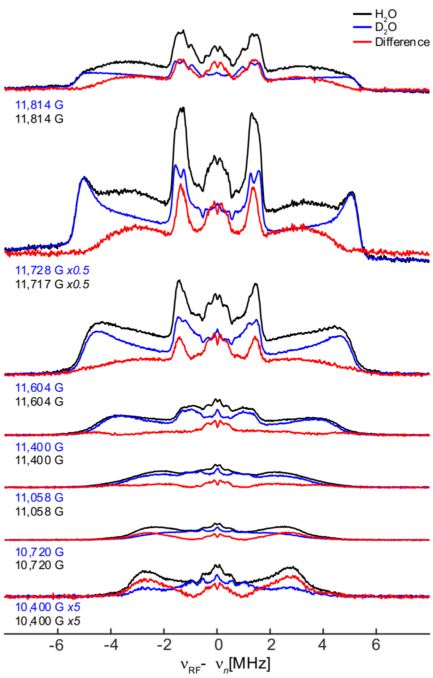

Figure S15. Q-band [1]H Davies ENDOR spectra of **Cu-V** for samples prepared in H_2O (black) and D_2O (blue). The subtraction of the two is depicted is shown in red. Spectrometer Conditions are listed in the Experimental Section and **Table S4**.

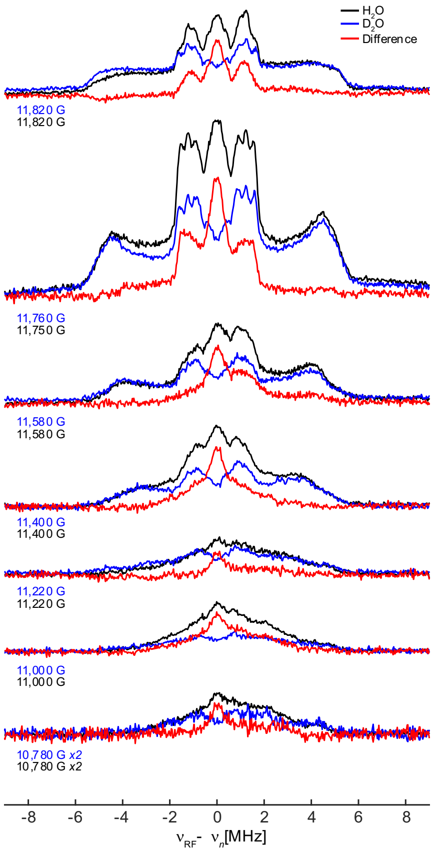

Figure S16. Q-band [1]H Davies ENDOR spectra of **Cu-VI** for samples prepared in H_2O (black) and D_2O (blue). The subtraction of the two is depicted is shown in red. Spectrometer Conditions are listed in the Experimental Section and **Table S4**.

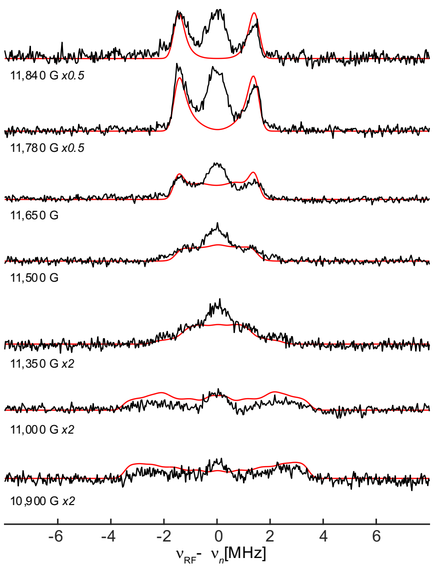

Figure S17. [1]H resonances of the exchangeable protons in **Cu-I** obtained through subtractions (**Figure S12**) in black with simulations in red. Simulation parameters are reported in **Table S12**. Spectrometer Conditions are listed in the Experimental Section and **Table S4**.

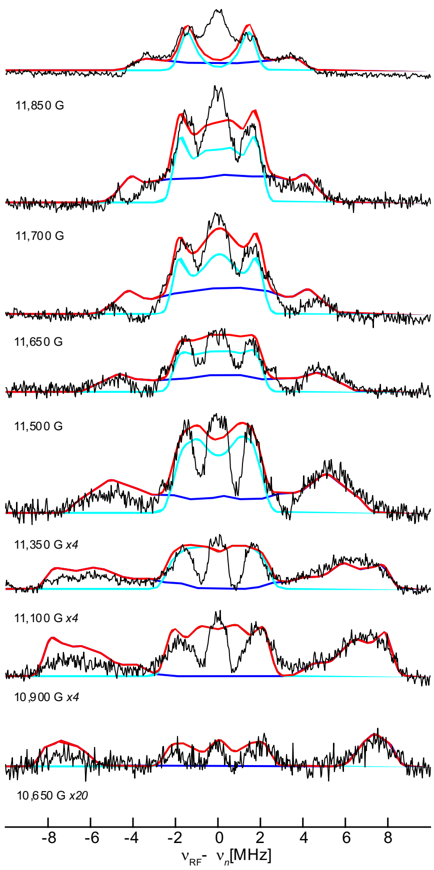

Figure S18. ^{1}H resonances of the exchangeable protons in **Cu-III** obtained through subtractions (**Figure S13**) in black. The simulations of the two individual nuclei are depicted in blue and cyan, with their sum in red. Simulation parameters are reported in **Table S12**. Spectrometer Conditions are listed in the Experimental Section and **Table S4**.

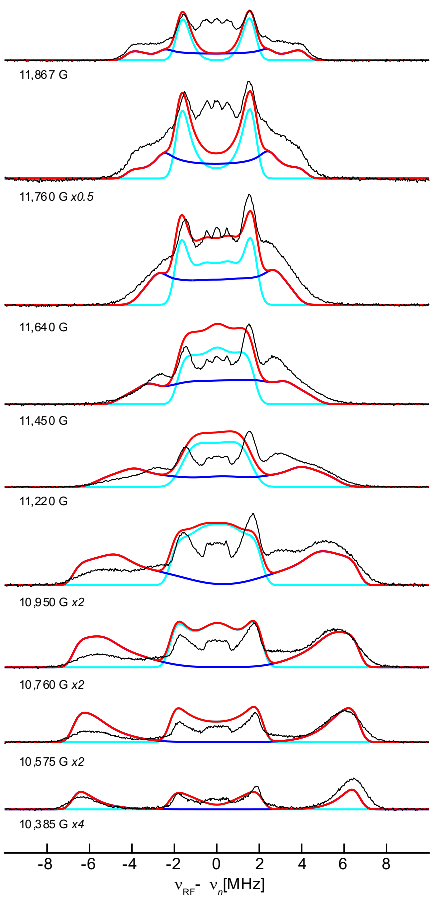

Figure S19. Q-band [1]H Davies ENDOR spectra of **Cu-IV** in black. The simulations of the two individual nuclei are depicted in blue and cyan, with their sum in red. Simulation parameters are reported in **Table S12**. Spectrometer Conditions are listed in the Experimental Section and **Table S4**.

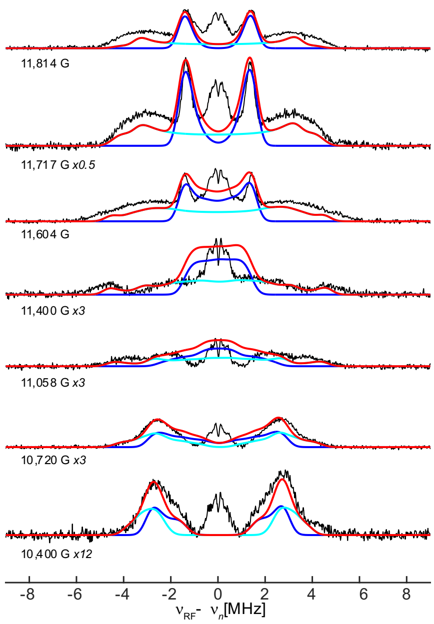

Figure S20. [1]H resonances of the exchangeable protons in **Cu-V** obtained through subtractions (**Figure S15**) in black. The simulations of the two individual nuclei are depicted in blue and cyan, with their sum in red. Simulation parameters are reported in **Table S12**. Spectrometer Conditions are listed in the Experimental Section and **Table S4**.

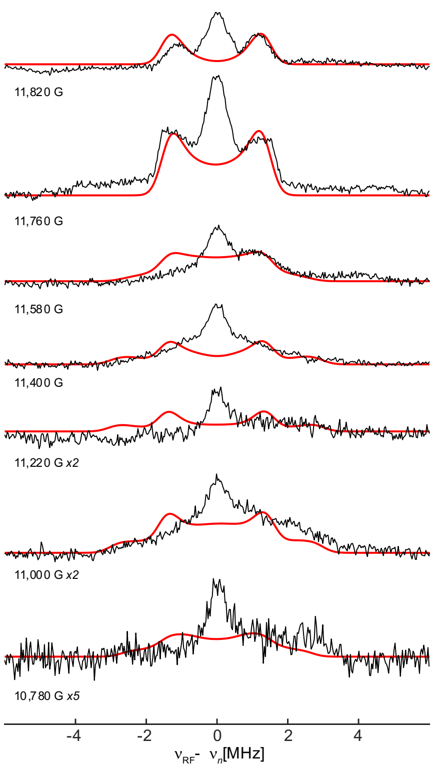

Figure S21. [1]H resonances of the exchangeable protons in **Cu-VI** obtained through subtractions (**Figure S16**) in black and simulations in red. Simulation parameters are reported in **Table S12**. Spectrometer Conditions are listed in the Experimental Section and **Table S4**.

Table S12. Summary of the Simulation Parameters for the ^{1}H ENDOR spectra (**Figures S17-S21**).

	$\mathbf{A}(^1\mathrm{H}) = [A_1, A_2, A_3]$ in MHz	Euler angles [a) $[\alpha, \beta, \gamma]$ in °	Linewidth (full width at half max) in mT	ExciteWidth in MHz
Cu-I	[+7, -3, -3]	[15, 0, 0]	0.4	200
Cu-III	[+4.9, -4.1, -3; -16.5, -8.0, +7.5]	[25, 0, 0; 0, 0, 0]	0.6	200
Cu-IV	[+4.3, -3.6, -3.4; -13.5, -5, +8.5]	[20, 0, 0; 0, 0, 0]	0.6	100 - 1000
Cu-V	[+6, -3, -3; -5.5, -9.5, +7.0]	[15, 0, 0; 30, 0, 0]	0.6	200
Cu-VI	[+6, -3, -2.8]	[50, 0, 0]	0.6	200

[a) The reported Euler angles describe the angles between the calculated **g**-tensor and the respective hyperfine tensor and are reported in a zyz' convention.

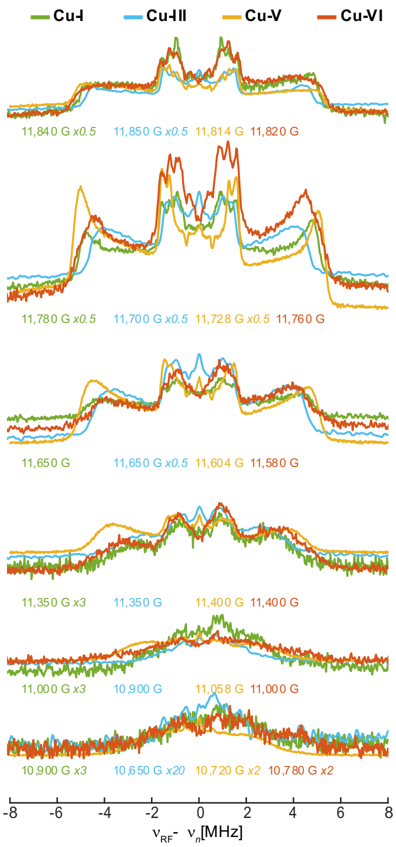

Figure S22. ^{1}H Davies ENDOR spectra of **Cu-I, Cu-III, Cu-V** and **Cu-VI** in D_2O showing only small differences in between the spectra, revealing only negligible differences of the bipyridine ligand upon pH changes and changes in the copper to bipyridine ratio. Spectrometer Conditions are listed in the Experimental Section.

Table S13. Summary of ^{1}H hyperfine couplings originating from H_xO ligands found in copper complexes and proteins.

	A = [A_1, A_2, A_3] in MHz	a_{iso} in MHz	**T** in MHz	Ref.
Axial waters				
$[Cu(H_2O)_6]^{2+}$ in Tutton salt; axial waters	[+7.79, -3.73, -3.55]	+0.17	[+7.62, -3.90, -3.72]	[1]
	[+7.27, -3.66, -3.24]	+0.12	[+7.15, -3.78, -3.36]	
Axial water in Amyloid beta peptide	A~3			[2]
Axial water in the octarepeat domain of the prion protein (can't exclude possibilities of other exchangeable protons)	n.r.[a)]	~0	t~2	[3]
axial water in $[Cu(H_2O)_6]^{2+}$ in mesoporous MCM-41	n.r.[a)]	1.7	2.2	[4]
Axial water in pMMO (Cu_B)	$A(g_\parallel)$~+10 MHz $A(g_\perp)$~-5 MHz	n.r.[a)]	n.r.[a)]	[5]
Two waters in trigonal bipyramidal LPMO	A_{max}~6	n.r.[a)]	n.r.[a)]	[6]
Equatorial waters / hydroxos				
$[Cu(H_2O)_6]^{2+}$ in Tutton salt; equatorial waters	[+9.19, -7.42, -4.71]	-0.98	[+10.17, -6.44, -3.73]	[1]
	[+9.23, -8.01, -4.07]	-0.95	[+10.18, -7.06, -3.12]	
	[+9.45, 8.89, 4.01]	-1.15	[+10.60, -7.74, -2.86]	
	[+9.98, -7.62, -3.50]	-0.38	[+10.36, -7.24, -3.12]	
Equatorial water in $[Cu(H_2O)_6]^{2+}$ in mesoporous MCM-41	n.r.[a)]	between 1.2 and 2.2	t~4.8	[4]
Equatorial water in bis(oxazoline) copper complex	[-10.8, -5.02, +8.6]	-2.41	n.r.[a)]	[7]
Equatorial waters in Cu(II) exchanged zeolites	[-5.5, -7.5, +8.5]	n.r.[a)]	n.r.[a)]	[8]
Equatorial hydroxo in LPMO	A_{max}~10.5	n.r.[a)]	n.r.[a)]	[6]
Equatorial hydroxo in zeolites	n.r.[a)]	-2.0	[-11.0, -2.5, +13.5]	[9]

a) Not reported.

Table S14. Summary of ^{17}O hyperfine couplings originating from H_xO ligands found in copper complexes and proteins.

	A = [A_1, A_2, A_3] in MHz / A measured at one field position	a_{iso} in MHz	**T** in MHz	Ref.
Axial waters				
Amyloid beta	1.5 ($g_\perp$)	n.r.[a)]	n.r.[a)]	2
Axial water in pMMO (Cu_B)	1.6 (g_2)	n.r.[a)]	n.r.[a)]	10
Axial water in pMMO (Cu_C)	3.6 (g_2)	n.r.[a)]	n.r.[a)]	10
Axial waters in $[Cu(H_2O)_6]^{2+}$	Unsplit at ^{17}O Larmor frequency [EDNMR]	n.r.[a)]	n.r.[a)]	11
Cu(II)-doped ^{17}O-water-enriched potassium zinc sulfate hexahydrate (Tutton salt) crystals	[0.13, 0.23, -3.81]	-1.15	[1.28, 1.38, -2.66]	12
Axial waters in Cu(II) exchanged zeolites	n.r.[a)]	-10.0 (hydrated)	[2.0, 2.0, -4.0] (hydrated)	8
Equatorial waters				
Equatorial waters in $[Cu(H_2O)_6]^{2+}$ in Tutton salt[b)]	~ [66, 30, 36]	48	n.r.[a)]	13
two types of equatorial waters in $^{63}Cu^{2+}$ doped zinc Tutton salt (along g_x / g_y)	[-33, -36, -63] MHz (g_x = 2.03) [-30, -48, -26] MHz (g_y = 2.15)	-44 -35	[11, 8, -19] [5, -13, 8]	14
Equatorial waters in Cu(II) exchanged zeolites	n.r.[a)]	-44.5 (hydrated) -51.0 (dehydrated-1) -41.0 (dehydrated-2)	[8.0, 8.0, -16.0] (hydrated) [12.0, 12.0, -24.0] (dehydrated-1) [9.5, 9.5, -19.0] (dehydrated-2)	8
Equatorial waters in Cu(II) exchanged zeolites	n.r.[a)]	-50 -51 (Framework)	[8, 8, -16] [7, 7, -14] (Framework)	15
equatorial waters in $[Cu(H_2O)_6]^{2+}$	~ 50 MHz [EDNMR]	n.r.[a)]	n.r.[a)]	11
Equatorial, organic ligands coordinating via ^{17}O nuclei				
Cu(II) picolinate:Zn(II) picolinate	[27, 29, 59]	n.r.[a)]	n.r.[a)]	16
Cu(II) hydroxyquinolate:phtalimide	[31, 33, 76]	n.r.[a)]	n.r.[a)]	17

a) Not reported.
b) First report, later refined and reported in reference [14].

^{14}N ENDOR

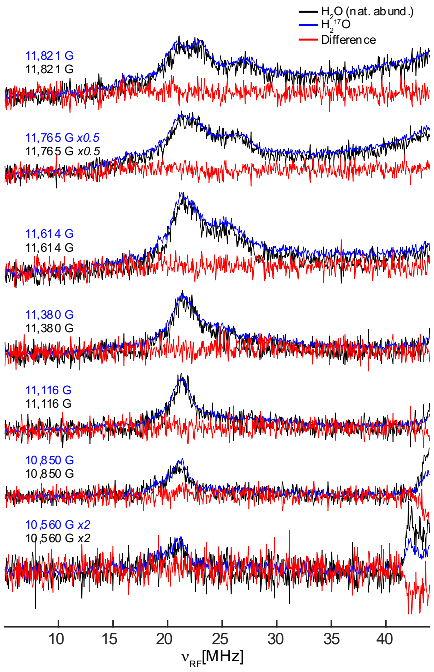

Figure S23. Q-band ^{14}N/^{17}O Davies ENDOR spectra of **Cu-I** for samples prepared in H_2O (natural abundance; black) and $H_2^{17}O$ (blue). The subtraction of the two is depicted is shown in red, revealing no ^{17}O resonances. Spectrometer Conditions are listed in the Experimental Section and **Table S5**.

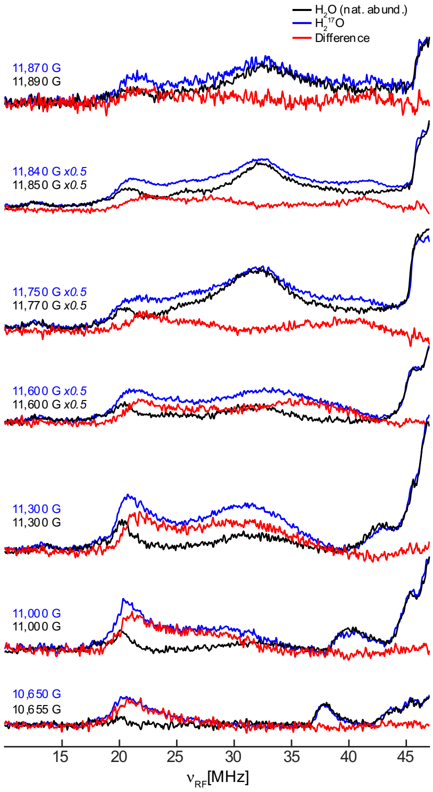

Figure S24. Q-band $^{14}N/^{17}O$ Davies ENDOR spectra of **Cu-III** for samples prepared in H_2O (natural abundance; black) and $H_2{}^{17}O$ (blue). The subtraction of the two is depicted is shown in red. Spectrometer Conditions are listed in the Experimental Section and **Table S5**.

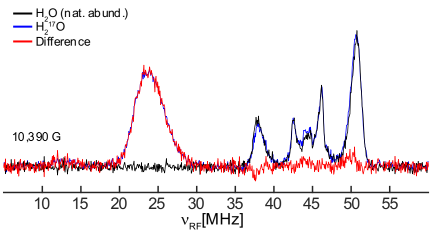

Figure S25. Q-band $^{14}N/^{17}O$ Davies ENDOR spectrum of **Cu-IV** for samples prepared in H_2O (natural abundance; black) and $H_2{}^{17}O$ (blue). The subtraction of the two is depicted is shown in red. The red difference spectrum and the black spectrum for a sample in regular water does not show any ^{14}N resonances, confirming the absence of the bipyridine ligand. Spectrometer Conditions are listed in the Experimental Section and **Table S5**.

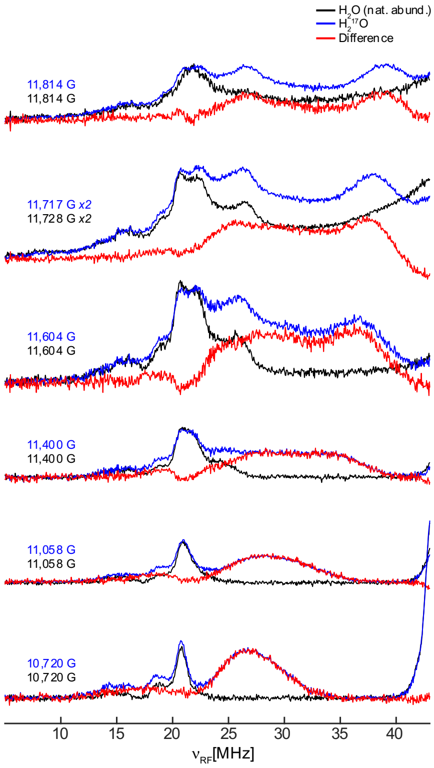

Figure S26. Q-band $^{14}N/^{17}O$ Davies ENDOR spectra of **Cu-V** for samples prepared in H_2O (natural abundance; black) and $H_2{}^{17}O$ (blue). The subtraction of the two is depicted is shown in red. Spectrometer Conditions are listed in the Experimental Section and **Table S5**.

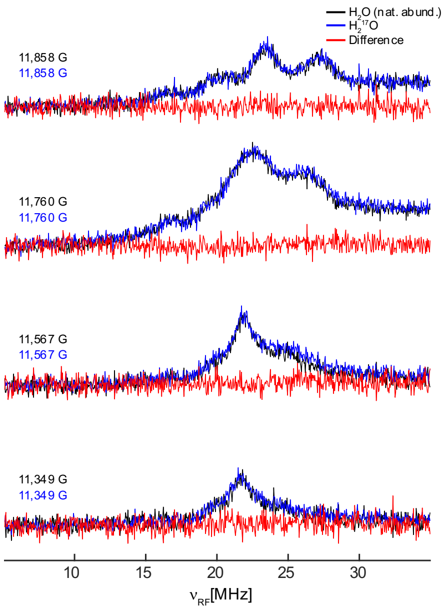

Figure S27. Q-band $^{14}N/^{17}O$ Davies ENDOR spectra of **Cu-VI** for samples prepared in H_2O (natural abundance; black) and $H_2{}^{17}O$ (blue). The subtraction of the two is depicted is shown in red, revealing no ^{17}O resonances. Spectrometer Conditions are listed in the Experimental Section and **Table S5**.

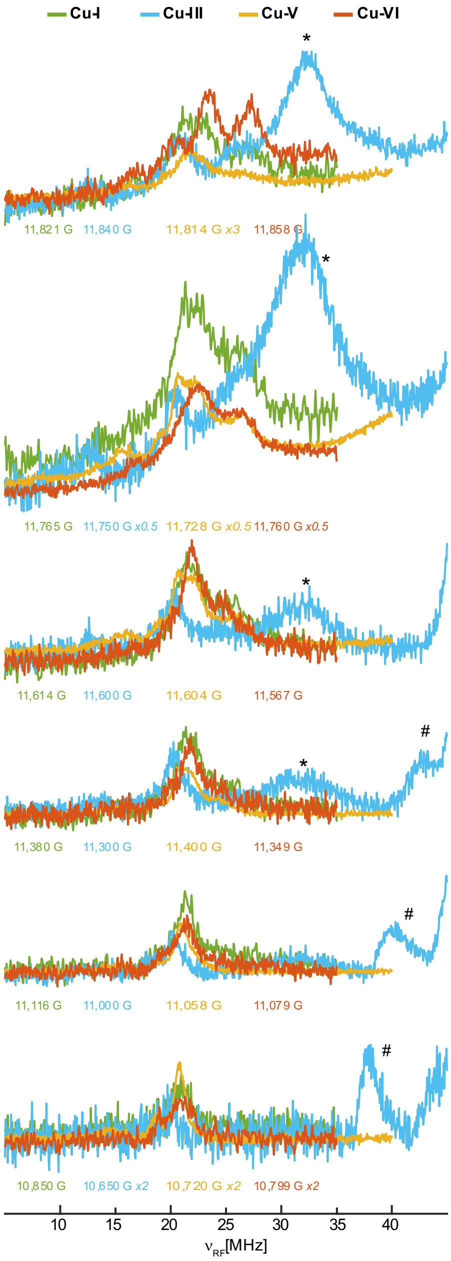

Figure S28. Q-band ^{14}N Davies ENDOR spectra of **Cu-I**, **Cu-III**, **Cu-V** and **Cu-VI** showing similar nitrogen couplings for all complexes. Signal intensities around 32 MHz (*) and above 35 MHz (#) are assigned to copper and proton resonances, respectively. Spectrometer Conditions are listed in the Experimental Section.

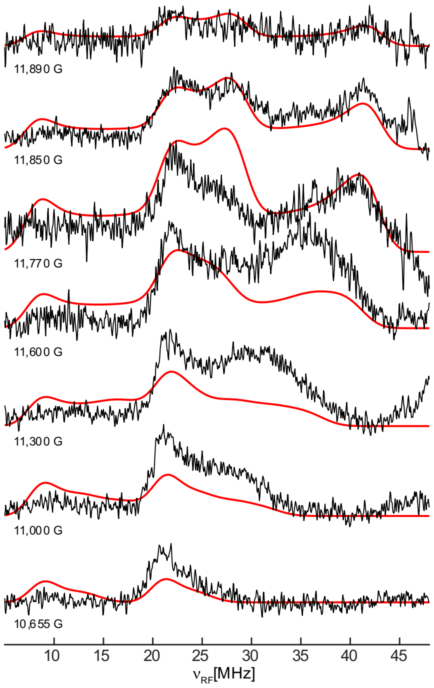

Figure S29. ^{17}O resonances of **Cu-III** obtained through subtractions (**Figure S24**) in black with simulations in red. Simulation parameters are reported in **Table S15**. Spectrometer Conditions are listed in the Experimental Section.

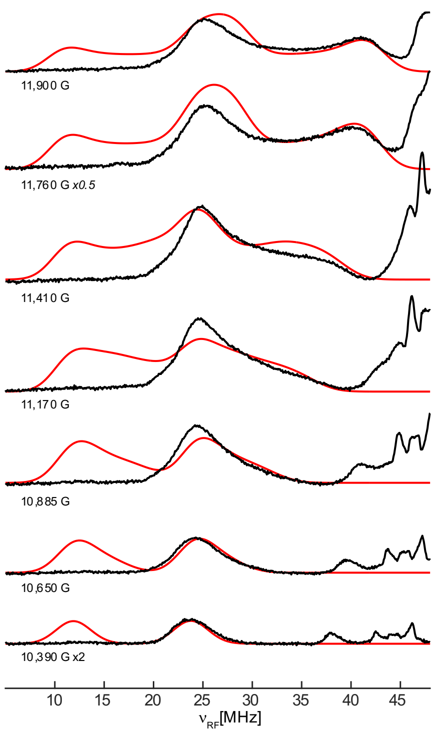

Figure S30. Q-band ^{17}O Davies ENDOR spectra of ^{17}O-enriched **Cu-IV** in black with simulations in red. Simulation parameters are reported in **Table S15**. Spectrometer Conditions are listed in the Experimental Section.

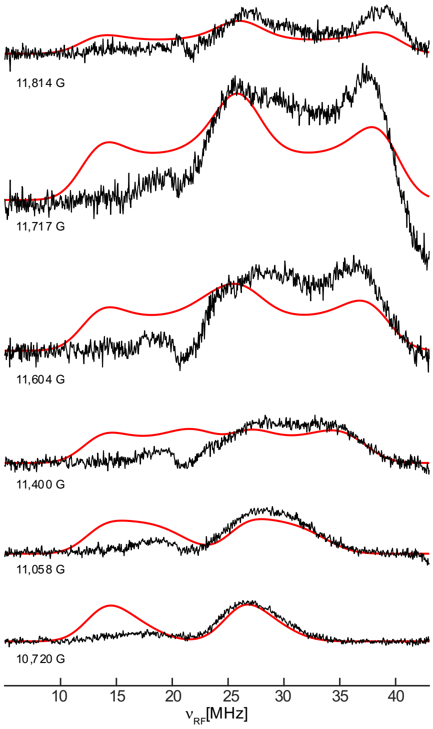

Figure S31. ^{17}O resonances of **Cu-V** obtained through subtractions (**Figure S26**) in black with simulations in red. Simulation parameters are reported in **Table S15**. Spectrometer Conditions are listed in the Experimental Section.

Table S15. Summary of the Simulation Parameters for the ^{14}N/ ^{17}O ENDOR spectra (**Figures S29-S31**).

	A(^{17}O) = [A_1, A_2, A_3] in MHz	Linewidth (full width at half max) in MHz	ExciteWidth in MHz
Cu-III	[-29, -72, -29; -29, -29, -72]	3	200
Cu-IV	[-34, -34, -70; -34, -70, -34]	4	200
Cu-V	[-39, -66, -39; -39, -39, -66]	4	200

EDNMR

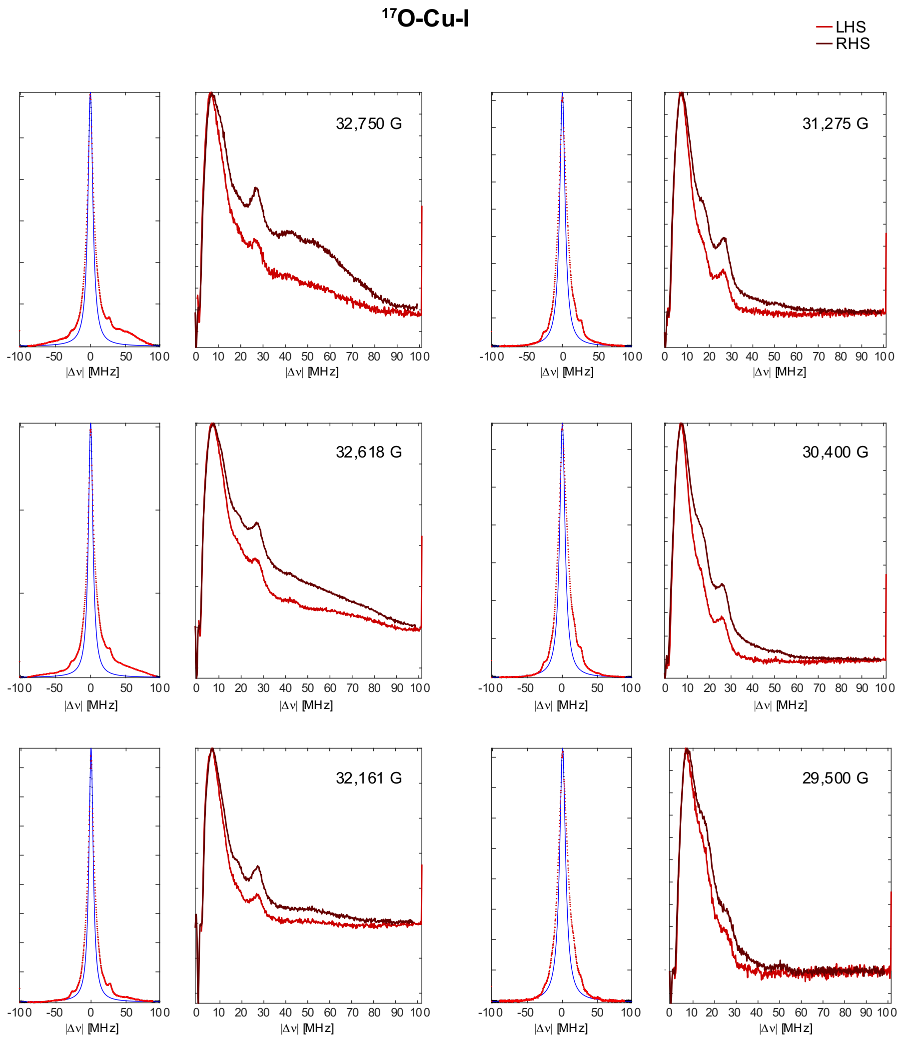

Figure S32. W-band EDNMR spectra of ^{17}O-enriched **Cu-I**, including the raw data with the fitted central hole in blue (left) and the processed data created through subtraction of both for the left-hand side (LHS) and right-hand side (RHS) (right). Spectrometer conditions are reported in the Experimental Section and **Table S7**.

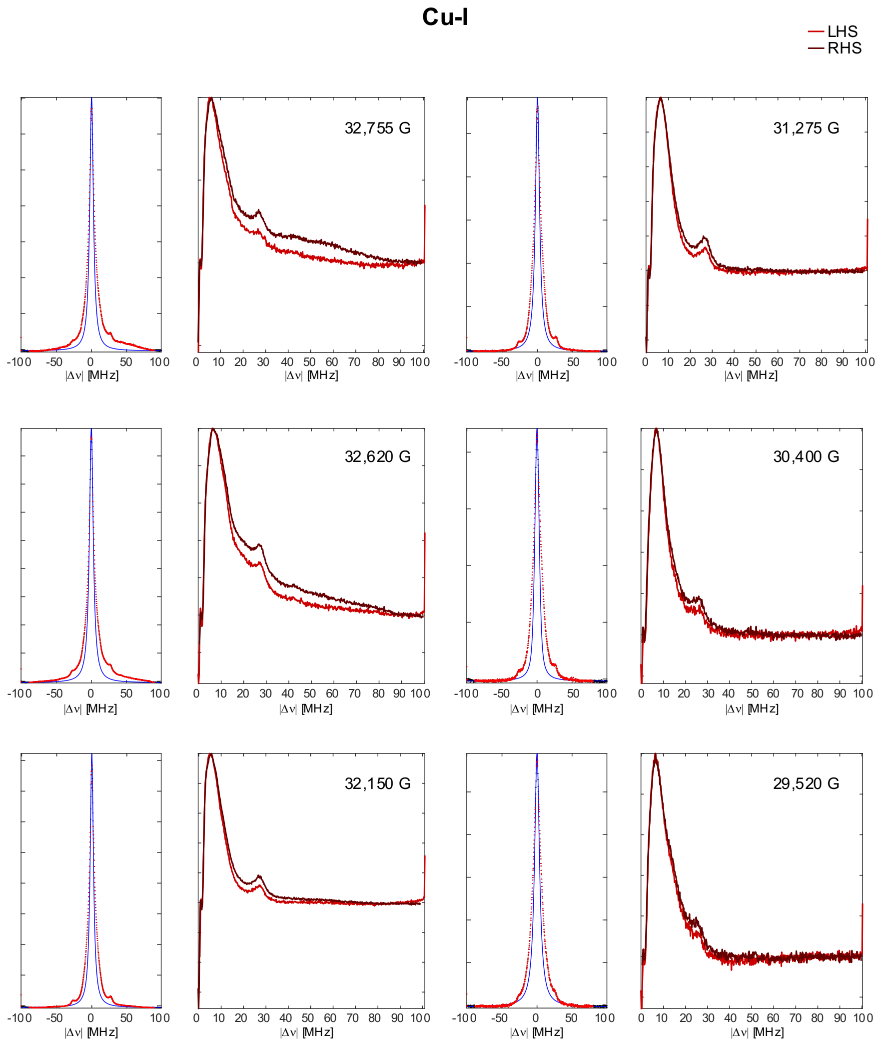

Figure S33. W-band EDNMR spectra of **Cu-I**, including the raw data with the fitted central hole in blue (left) and the processed data created through subtraction of both for the LHS and RHS (right). Spectrometer conditions are reported in the Experimental Section and **Table S7**.

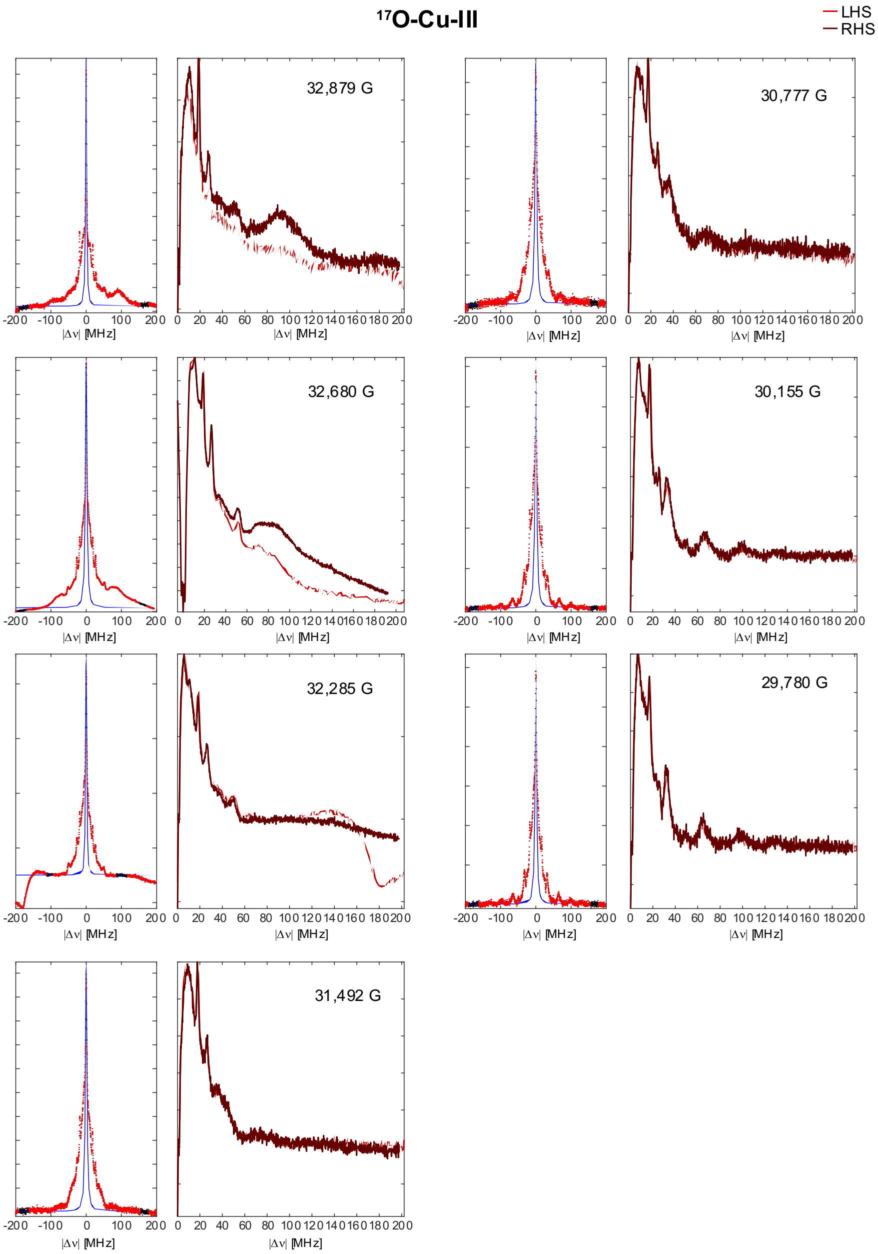

Figure S34. W-band EDNMR spectra of ^{17}O-enriched **Cu-III**, including the raw data with the fitted central hole in blue (left) and the processed data created through subtraction of both for the LHS and RHS (right). Spectrometer conditions are reported in the Experimental Section and **Table S7**.

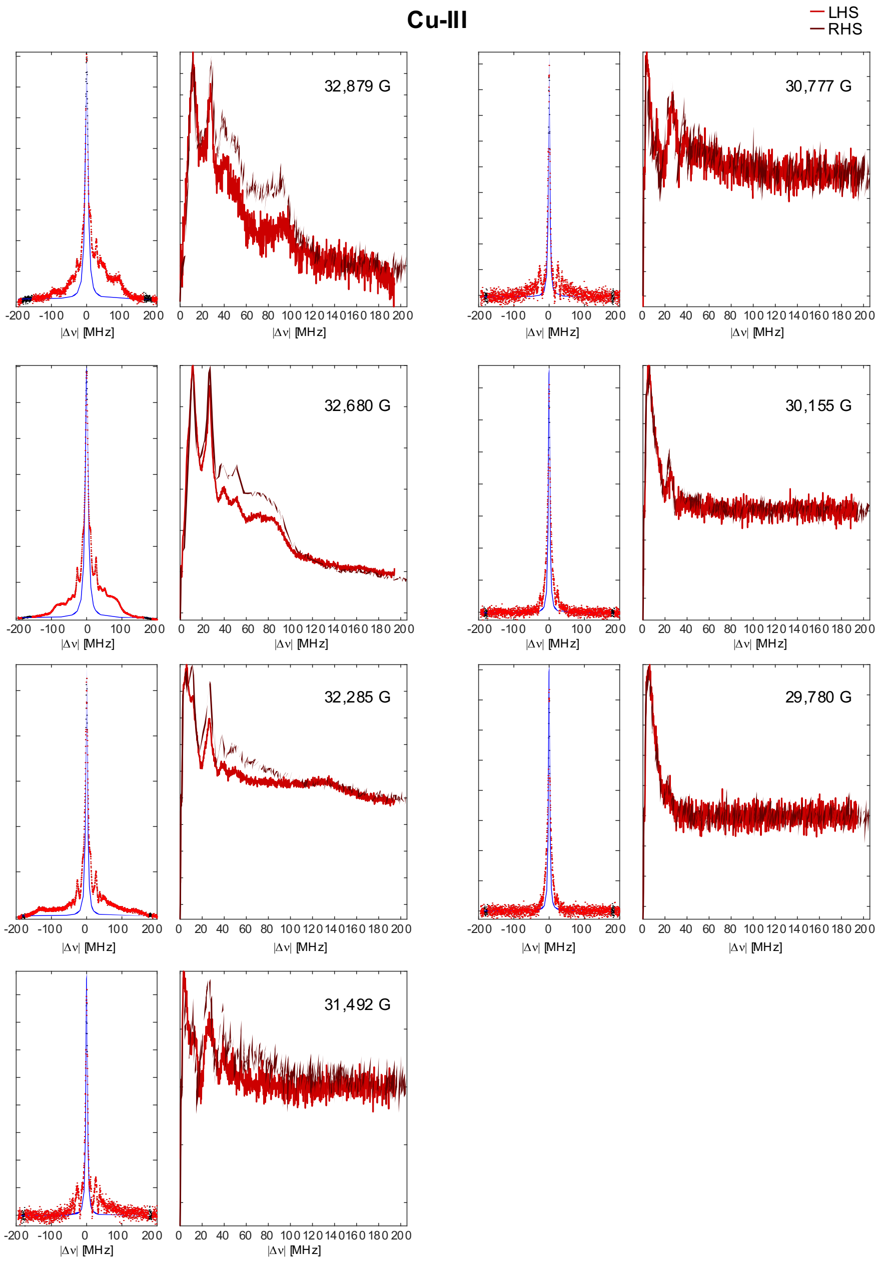

Figure S35. W-band EDNMR spectra of **Cu-III**, including the raw data with the fitted central hole in blue (left) and the processed data created through subtraction of both for the LHS and RHS (right). Spectrometer conditions are reported in the Experimental Section and **Table S7**.

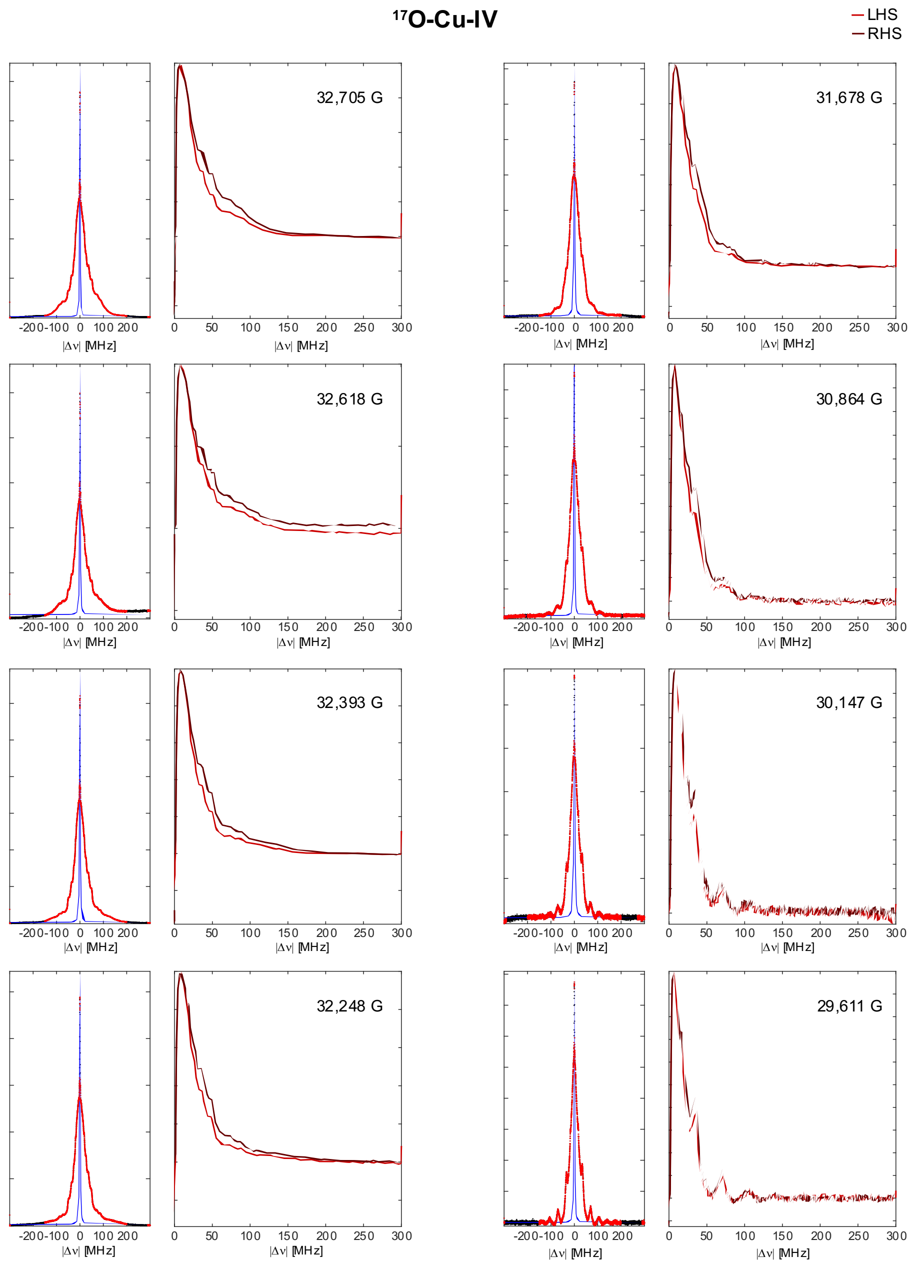

Figure S36. W-band EDNMR spectra of ^{17}O-enriched **Cu-IV**, including the raw data with the fitted central hole in blue (left) and the processed data created through subtraction of both for the LHS and RHS (right). Spectrometer conditions are reported in the Experimental Section and **Table S7**.

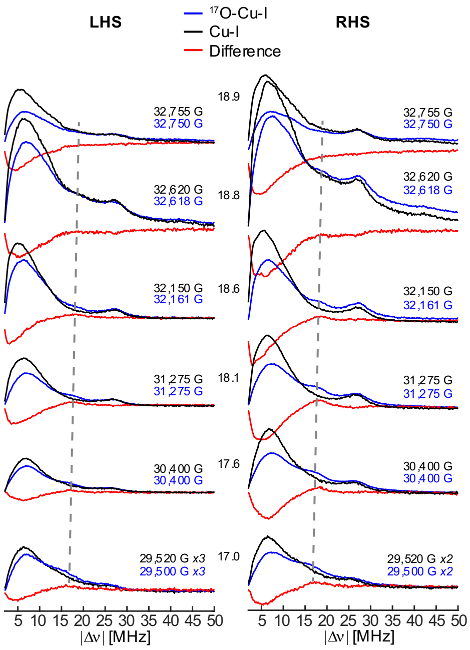

Figure S37. Processed W-band EDNMR spectra of **Cu-I** (black) and ^{17}O-enriched **Cu-I** (blue), obtained as shown in **Figure S32** and **S33**. Subsequent subtraction of both spectra (red) yields intensity mostly on the ^{17}O Larmor frequency (grey, dashed lines), indicating the axial coordination of water molecules.

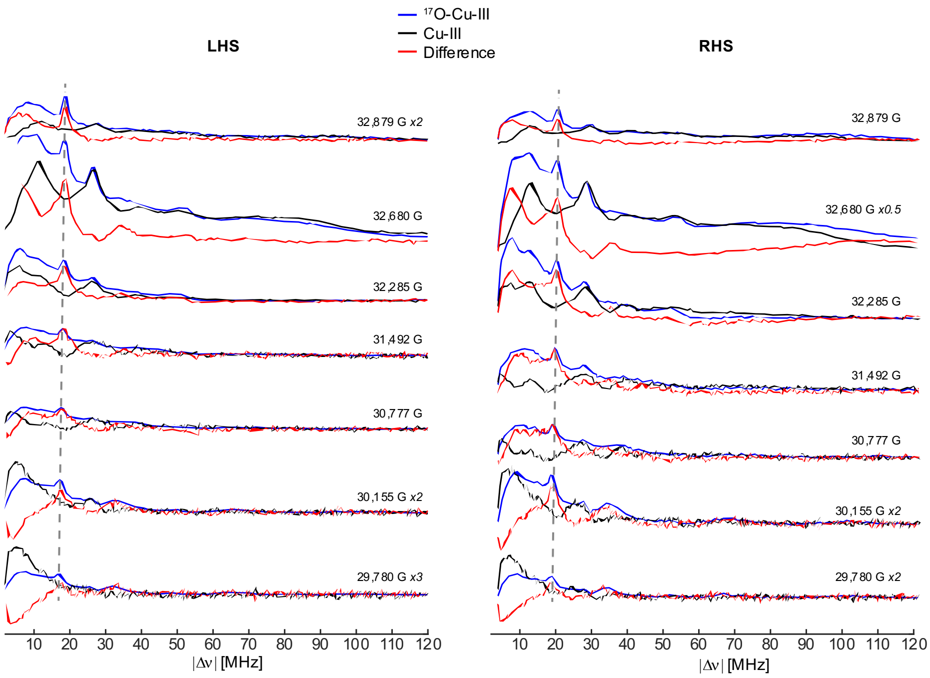

Figure S38. Processed W-band EDNMR spectra of **Cu-III** (black) and ^{17}O-enriched **Cu-III** (blue), obtained as shown in **Figure S34** and **S35**. Subsequent subtraction of both spectra (red) yields the ^{17}O resonances of equatorial H_xO ligands and axial waters, as seen mostly as intensity on the ^{17}O Larmor frequency (grey, dashed lines).

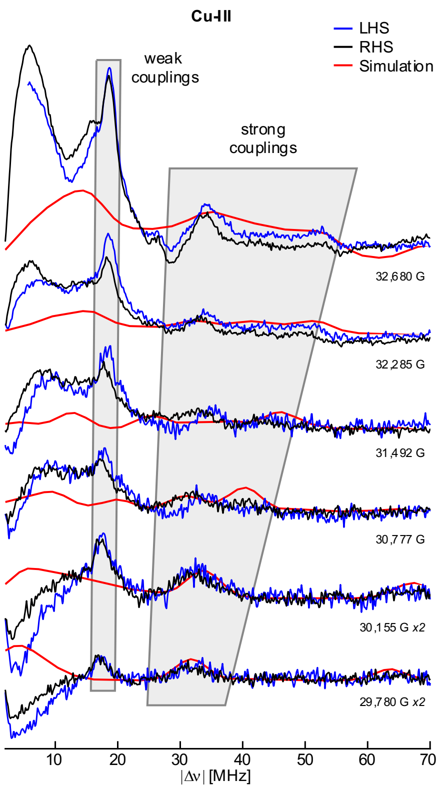

Figure S39. ^{17}O resonances of ^{17}O-enriched **Cu-III**, obtained through W-band EDNMR subtractions (**Figure S38**) in blue (LHS) and black (RHS), together with simulations of the strongly coupled, equatorial ^{17}O nuclei. Simulations were obtained for a single ^{17}O nucleus with couplings of [-29, -72, -29] MHz, without considering the copper hyperfine with the following simulation parameters: 6 MHz gaussian broadening, 200 MHz excitation width, GridSize: 20. Intensity on the ^{17}O Larmor frequency, indicating axial water coordination, is marked by a grey, dashed line.

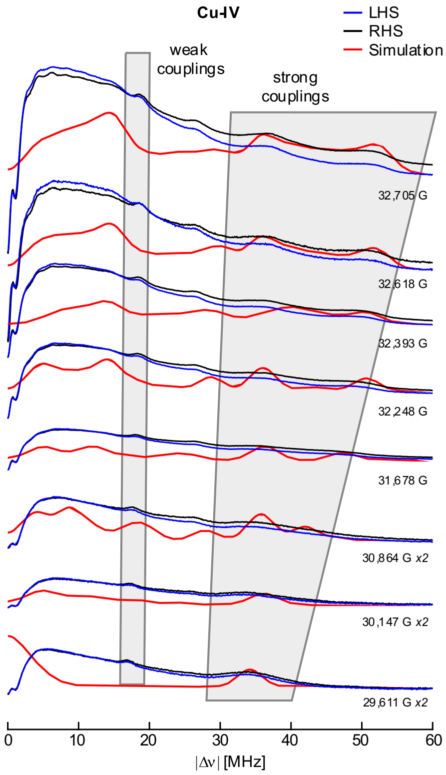

Figure S40. ^{17}O resonances of ^{17}O-enriched **Cu-IV**, obtained through W-band EDNMR spectroscopy (**Figure S36**) in blue (LHS) and black (RHS), together with simulations of the strongly coupled, equatorial ^{17}O nuclei. Simulations were obtained for a single ^{17}O nucleus with couplings of [-34, -70, -34] MHz, without considering the copper hyperfine with the following simulation parameters: 4 MHz gaussian broadening, 200 MHz excitation width, GridSize: 20. Intensity on the ^{17}O Larmor frequency, indicating axial water coordination, is marked by a grey, dashed line.

Computational Studies

Table S16. Calculated EPR parameters of copper bpy complexes **DFT-I**, **DFT-II**, **DFT-III** and **DFT-IV**.

	g = [g_1, g_2, g_3]	**A** = [A_1, A_2, A_3] in MHz		
		^{63}Cu	^{1}H [a)]	^{17}O
DFT-I	[2.179, 2.056, 2.054]	[-686, -56, -44]	[-7.7, +9.0, -3.1] [-6.1, +7.2, -9.6] [-10.4, -4.5, +7.8] [-3.5, -7.8, +9.3]	[-34, -61, -35] [-36, -37, -64]
DFT-II	[2.195, 2.064, 2.063]	[-644, 13, -0.3]	*equatorial*: [-8.0, +8.2, -3.9] [-5.8, +7.2, -9.6] [-11.1, -5.1, +7.3] [-4.8, -8.9, +8.1] *axial*: [+5.2, -2.4, -2.4] [+5.7, -2.8, -2.7] [+6.0, -2.8, -2.9] [+6.0, -2.9, -2.7]	*equatorial*: [-32, -32, -59] [-31, -56, -32] *axial:* [1.0, 2.5, 2.4] [1.2, 2.7, 2.8]
DFT-III	[2.148, 2.046, 2.042]	[-725, -108, -119]	[-22.3, -10.8, +7.4] [-22.3, -10.8, +7.4]	[-20, -81, -20] [-20, -81, -20]
DFT-IV	[2.176, 2.051, 2.048]	[-718, -110, -114]	[-16.4, -7.2, +7.8] [-16.3, -7.1, +7.8] [-16.4, -7.2, +7.8] [-16.3, -7.1, +7.8]	[-30, -73, -29] [-30, -73, -29] [-29, -72, -29] [-29, -72, -29]

[a)] Only the hyperfine couplings of the exchangeable protons are reported.

Coordinates of DFT Optimized Structures

DFT-I

Cu	0.000000000000	0.000000000000	0.000000000000
O	1.973553000000	-0.212414000000	0.357290000000
O	0.131284000000	-1.871263000000	-0.736136000000
N	-1.957267000000	0.000000000000	0.000000000000
N	-0.224156000000	1.897573000000	0.418548000000
C	-2.737893000000	-1.072606000000	-0.196844000000
C	-4.705908000000	0.269080000000	0.093036000000
C	-4.126806000000	-0.974290000000	-0.156747000000
C	-3.887278000000	1.377797000000	0.304213000000
C	-2.502486000000	1.217554000000	0.256193000000
C	-1.524406000000	2.291244000000	0.477142000000
C	-1.852523000000	3.623314000000	0.727736000000
C	-0.830285000000	4.552583000000	0.913562000000
C	0.763413000000	2.788856000000	0.594088000000
C	0.497004000000	4.132700000000	0.844027000000
H	1.783820000000	2.416102000000	0.529449000000
H	2.264143000000	0.106897000000	1.234920000000
H	2.557945000000	0.217557000000	-0.298996000000
H	1.042831000000	-2.204827000000	-0.607507000000
H	-0.018147000000	-1.881400000000	-1.703877000000
H	-2.231934000000	-2.018545000000	-0.382438000000
H	-4.731790000000	-1.864769000000	-0.319544000000
H	-5.789741000000	0.378548000000	0.127910000000
H	-4.322278000000	2.354828000000	0.506050000000
H	-2.894919000000	3.932303000000	0.775028000000
H	-1.072018000000	5.597154000000	1.109150000000
H	1.325465000000	4.825834000000	0.980539000000

DFT-II

Cu	0.000000000000	0.000000000000	0.000000000000
O	-2.048678000000	0.123539000000	-0.067195000000
O	0.072441000000	-0.742110000000	-2.344239000000
O	-0.208870000000	-0.152889000000	2.394994000000
O	-0.351740000000	-2.017951000000	0.127873000000
N	1.978913000000	0.000000000000	0.000000000000
N	0.253945000000	1.956283000000	-0.014004000000
C	-0.727145000000	2.870225000000	0.004994000000
C	2.768724000000	-1.084045000000	-0.002376000000
C	-0.453222000000	4.235725000000	0.016772000000
C	0.876959000000	4.653905000000	0.013179000000
C	1.892936000000	3.700158000000	0.004029000000
C	4.157579000000	-0.980002000000	-0.001296000000
C	1.554805000000	2.345630000000	-0.007939000000
C	2.526581000000	1.243553000000	-0.004936000000
C	3.912139000000	1.412929000000	-0.002709000000
C	4.735272000000	0.288762000000	0.001013000000

H	5.818913000000	0.405361000000	0.004154000000
H	4.343609000000	2.412050000000	-0.003192000000
H	4.763034000000	-1.885022000000	-0.001487000000
H	2.275720000000	-2.054353000000	-0.009247000000
H	1.125121000000	5.715148000000	0.021176000000
H	-1.276533000000	4.948223000000	0.029795000000
H	0.067180000000	-2.472479000000	0.883906000000
H	-0.051562000000	-2.467539000000	-0.687265000000
H	-2.387371000000	-0.779394000000	0.101810000000
H	-2.367062000000	0.348093000000	-0.964707000000
H	-1.748095000000	2.493138000000	0.018257000000
H	-0.701561000000	-0.452036000000	-2.861291000000
H	0.824926000000	-0.273256000000	-2.749731000000
H	0.620666000000	0.212391000000	2.755079000000
H	-0.887801000000	0.496474000000	2.656972000000
H	2.937071000000	4.007029000000	0.006867000000

DFT-III

Cu	0.000000000000	0.000000000000	0.000000000000
O	0.310437000000	-1.874727000000	-0.046214000000
O	-1.882934000000	-0.038033000000	-0.255736000000
N	1.957654000000	0.355009000000	0.353364000000
N	0.000000000000	2.019218000000	0.000000000000
C	-1.091335000000	2.775769000000	-0.187831000000
C	-1.034195000000	4.167767000000	-0.175243000000
C	0.198453000000	4.786252000000	0.043543000000
C	1.331229000000	3.998592000000	0.241647000000
C	1.202403000000	2.607025000000	0.212822000000
C	2.317747000000	1.660532000000	0.403133000000
C	3.647294000000	2.035286000000	0.617558000000
C	4.610202000000	1.041629000000	0.785866000000
C	4.225242000000	-0.299581000000	0.734006000000
C	2.883395000000	-0.602214000000	0.512566000000
H	2.503230000000	-1.622822000000	0.450840000000
H	-1.941237000000	4.749940000000	-0.333557000000
H	-2.014751000000	2.217324000000	-0.347152000000
H	-2.181405000000	-0.964334000000	-0.250485000000
H	-0.527989000000	-2.327839000000	-0.243600000000
H	0.279084000000	5.873357000000	0.061146000000
H	2.301143000000	4.461021000000	0.416924000000
H	3.928601000000	3.086550000000	0.650616000000
H	5.652268000000	1.314100000000	0.954721000000
H	4.949600000000	-1.103227000000	0.861157000000

DFT-IV

Cu	0.000000000000	0.000000000000	0.000000000000
O	-0.000001000000	-1.973841000000	-0.000003000000
O	0.000000000000	1.973842000000	0.000000000000
O	1.961657000000	0.082212000000	0.137943000000

O	-1.961656000000	-0.082212000000	-0.137945000000
H	-0.925328000000	2.248859000000	-0.122853000000
H	-2.279514000000	0.837061000000	-0.107060000000
H	0.925326000000	-2.248859000000	0.122851000000
H	2.279513000000	-0.837061000000	0.107058000000

thf-I

Cu	0.000000000000	0.000000000000	0.000000000000
O	-1.973550000000	0.121420000000	0.237001000000
H	-2.215027000000	0.317476000000	1.165747000000
H	-2.405185000000	-0.730899000000	0.023742000000
O	-0.242713000000	-1.865572000000	-0.557727000000
O	1.963901000000	0.000000000000	0.000000000000
O	0.185886000000	1.946973000000	0.274351000000
C	0.350286000000	-2.352985000000	-1.829215000000
H	1.179928000000	-1.687827000000	-2.095542000000
C	0.763784000000	-3.789977000000	-1.547453000000
H	1.808452000000	-3.835039000000	-1.209574000000
C	-0.186826000000	-4.215900000000	-0.416369000000
H	-1.177105000000	-4.476292000000	-0.815472000000
C	-0.273858000000	-2.963536000000	0.434568000000
H	-1.207022000000	-2.846134000000	0.996960000000
C	2.804649000000	-1.083837000000	0.532848000000
H	2.627361000000	-1.114208000000	1.613558000000
C	4.208071000000	-0.689479000000	0.111542000000
H	4.877411000000	-1.557926000000	0.084297000000
C	3.969274000000	-0.077816000000	-1.278254000000
H	4.791473000000	0.570693000000	-1.604174000000
C	2.682506000000	0.710395000000	-1.090654000000
H	-0.446126000000	-2.270588000000	-2.579742000000
H	0.662276000000	-4.416067000000	-2.442131000000
H	0.198009000000	-5.065712000000	0.160263000000
H	0.587724000000	-2.851331000000	1.107372000000
H	2.498716000000	-2.032548000000	0.070854000000
H	4.621605000000	0.057884000000	0.803203000000
H	3.829205000000	-0.871486000000	-2.025592000000
H	2.848555000000	1.733034000000	-0.729550000000
C	-0.761747000000	2.901073000000	-0.346411000000
C	0.484369000000	2.378427000000	1.662544000000
C	-1.261835000000	3.758444000000	0.802050000000
C	-0.043919000000	3.800566000000	1.738100000000
H	-0.048530000000	1.700871000000	2.345219000000
H	1.566716000000	2.272400000000	1.794119000000
H	0.707275000000	4.510744000000	1.364369000000
H	-0.305873000000	4.073922000000	2.767480000000
H	-2.116474000000	3.277295000000	1.299016000000
H	-1.569243000000	4.753986000000	0.459085000000
H	-0.173214000000	3.472143000000	-1.078156000000
H	-1.534288000000	2.318841000000	-0.859246000000
H	2.027906000000	0.724599000000	-1.970113000000

thf-II

Cu	0.000000000000	0.000000000000	0.000000000000
O	0.154013000000	-1.988698000000	-0.089442000000
O	-1.986546000000	-0.200137000000	-0.063199000000
H	-2.272588000000	-0.789274000000	-0.791857000000
H	-2.380257000000	0.673780000000	-0.265983000000
H	-0.538814000000	-2.455077000000	0.421253000000
H	1.004920000000	-2.260094000000	0.312632000000
O	1.959178000000	0.000000000000	0.000000000000
O	-0.303393000000	1.922781000000	0.140842000000
C	2.656319000000	-0.058787000000	-1.320173000000
H	1.942507000000	0.261604000000	-2.088776000000
C	3.865010000000	0.847929000000	-1.159188000000
H	3.615316000000	1.877911000000	-1.450125000000
C	4.155261000000	0.774994000000	0.348658000000
H	4.666963000000	-0.162727000000	0.606554000000
C	2.761755000000	0.803053000000	0.946197000000
H	2.652630000000	0.325513000000	1.925736000000
C	-0.420831000000	2.570228000000	1.468954000000
H	-1.325626000000	2.161512000000	1.932137000000
C	-0.473618000000	4.048222000000	1.133694000000
H	-0.166981000000	4.662654000000	1.988890000000
C	0.497107000000	4.157413000000	-0.053263000000
H	0.329740000000	5.058943000000	-0.654796000000
C	0.210855000000	2.898124000000	-0.856440000000
H	1.094501000000	2.463359000000	-1.336458000000
H	2.920326000000	-1.113793000000	-1.467490000000
H	4.706424000000	0.502962000000	-1.772062000000
H	4.757366000000	1.619374000000	0.705545000000
H	2.356929000000	1.823700000000	0.970243000000
H	0.463487000000	2.307640000000	2.066173000000
H	-1.491494000000	4.335244000000	0.834963000000
H	1.537619000000	4.159129000000	0.300491000000
H	-0.592802000000	3.022785000000	-1.593002000000

thf-III

Cu	0.000000000000	0.000000000000	0.000000000000
O	-1.981980000000	0.017625000000	0.115761000000
O	1.987731000000	0.000000000000	0.000000000000
H	2.313277000000	-0.921198000000	0.072565000000
H	2.367825000000	0.350585000000	-0.831772000000
H	-2.414541000000	-0.459153000000	-0.622342000000
H	-2.296520000000	0.943646000000	0.056655000000
O	-0.080019000000	1.968521000000	-0.049592000000
O	0.083453000000	-1.958983000000	0.200562000000
C	0.699591000000	2.736493000000	0.959128000000
H	1.264131000000	2.014579000000	1.559273000000

C	1.544471000000	3.697334000000	0.145122000000
H	2.476328000000	3.212205000000	-0.178528000000
C	0.639896000000	3.994320000000	-1.060613000000
H	-0.150460000000	4.706637000000	-0.785071000000
C	0.044187000000	2.633220000000	-1.374282000000
H	-0.962952000000	2.649571000000	-1.805466000000
H	-0.045676000000	3.245593000000	1.585176000000
H	1.795422000000	4.597710000000	0.719132000000
H	1.192310000000	4.393343000000	-1.919939000000
H	0.712592000000	2.021825000000	-1.996764000000
C	-0.696803000000	-2.578724000000	1.304523000000
C	-0.072255000000	-2.782550000000	-1.031331000000
C	-1.582421000000	-3.605496000000	0.624989000000
C	-0.707346000000	-4.074323000000	-0.547363000000
H	-0.725130000000	-2.228497000000	-1.720575000000
H	0.930680000000	-2.884411000000	-1.460529000000
H	0.063745000000	-4.775717000000	-0.198942000000
H	-1.286487000000	-4.554630000000	-1.345401000000
H	-2.506092000000	-3.136087000000	0.257069000000
H	-1.849490000000	-4.421432000000	1.307629000000
H	0.045279000000	-3.031391000000	1.976332000000
H	-1.230870000000	-1.774324000000	1.821649000000

thf-IV

Cu	0.000000000000	0.000000000000	0.000000000000
O	1.985949000000	0.000000000000	0.000000000000
O	-1.973849000000	-0.142518000000	-0.155525000000
O	0.012084000000	-1.966056000000	-0.255711000000
H	2.361725000000	-0.493556000000	0.758931000000
H	2.286840000000	0.925825000000	0.117403000000
H	-2.463443000000	0.379356000000	0.512837000000
H	-2.309233000000	0.155893000000	-1.026174000000
H	0.659046000000	-2.443954000000	0.302292000000
H	-0.864157000000	-2.331061000000	-0.013163000000
O	0.116274000000	1.941609000000	0.199029000000
H	0.365952000000	3.389602000000	-1.264293000000
H	-1.643789000000	4.635294000000	-0.627705000000
H	-1.474334000000	4.188791000000	2.044634000000
H	-0.928626000000	1.835748000000	2.021361000000
C	-0.475853000000	2.818870000000	-0.848579000000
H	-0.900741000000	2.169501000000	-1.621912000000
C	-1.468142000000	3.687388000000	-0.104448000000
H	-2.428116000000	3.164250000000	0.013138000000
C	-0.778681000000	3.879849000000	1.255185000000
H	0.023552000000	4.627081000000	1.178406000000
C	-0.199841000000	2.504418000000	1.543064000000
H	0.741441000000	2.499475000000	2.103647000000

thf-V

Cu	0.000000000000	0.000000000000	0.000000000000
O	-1.830147000000	-0.176203000000	0.172909000000
H	-2.176716000000	0.610813000000	0.631280000000
O	0.054060000000	1.981587000000	0.379668000000
O	0.060529000000	-1.938898000000	-0.658610000000
O	1.997233000000	0.000000000000	0.000000000000
C	1.033174000000	-2.323330000000	-1.696254000000
H	1.585066000000	-1.424210000000	-1.987334000000
C	1.887781000000	-3.407646000000	-1.063279000000
H	2.703281000000	-2.960052000000	-0.477262000000
C	0.881867000000	-4.114306000000	-0.142421000000
H	0.241727000000	-4.793341000000	-0.723671000000
C	0.065392000000	-2.955221000000	0.412580000000
H	-0.981219000000	-3.197853000000	0.630205000000
C	2.675730000000	-0.267368000000	1.287303000000
H	1.946600000000	-0.115398000000	2.093519000000
C	3.857012000000	0.693156000000	1.326456000000
H	4.709332000000	0.262258000000	1.865834000000
C	4.150859000000	0.937955000000	-0.162000000000
H	4.714293000000	1.862754000000	-0.337271000000
C	2.755009000000	1.009180000000	-0.753688000000
H	2.684783000000	0.728743000000	-1.811610000000
H	0.450798000000	-2.697642000000	-2.551296000000
H	2.323002000000	-4.077727000000	-1.815224000000
H	1.362976000000	-4.688010000000	0.659507000000
H	0.533527000000	-2.511480000000	1.302991000000
H	2.983289000000	-1.321483000000	1.262606000000
H	3.572338000000	1.634558000000	1.817491000000
H	4.710729000000	0.095539000000	-0.592933000000
H	2.284708000000	1.989111000000	-0.590990000000
C	-0.811153000000	2.890704000000	-0.402499000000
C	0.090322000000	2.424847000000	1.788007000000
C	-1.529142000000	3.739159000000	0.633991000000
C	-0.492933000000	3.828406000000	1.764540000000
H	-0.521935000000	1.727985000000	2.378425000000
H	1.136495000000	2.370944000000	2.111348000000
H	0.285809000000	4.564253000000	1.517970000000
H	-0.936682000000	4.096260000000	2.731385000000
H	-2.437231000000	3.228019000000	0.986240000000
H	-1.811658000000	4.720277000000	0.232844000000
H	-0.141755000000	3.482390000000	-1.043068000000
H	-1.468540000000	2.268707000000	-1.020175000000

thf-VI

Cu	0.000000000000	0.000000000000	0.000000000000
O	1.875686000000	0.000000000000	0.000000000000
O	-0.322223000000	-1.852170000000	0.082221000000
H	0.534411000000	-2.313851000000	0.121892000000
H	2.184723000000	-0.923332000000	0.009578000000
O	-0.017876000000	2.105298000000	-0.044719000000

O	-2.037117000000	0.344809000000	0.012976000000
C	-0.499084000000	2.667802000000	-1.302242000000
H	-0.997611000000	3.626198000000	-1.079337000000
C	0.765714000000	2.864685000000	-2.124187000000
H	0.630656000000	3.603788000000	-2.924133000000
C	1.801729000000	3.310800000000	-1.066325000000
H	2.783893000000	2.859415000000	-1.251861000000
C	1.206438000000	2.838837000000	0.276161000000
H	1.849179000000	2.142258000000	0.821320000000
C	-2.594822000000	0.702387000000	1.326597000000
H	-1.809209000000	0.556780000000	2.078822000000
C	-3.806637000000	-0.201919000000	1.510841000000
H	-4.572576000000	0.262944000000	2.144218000000
C	-4.273188000000	-0.426758000000	0.064664000000
H	-4.905531000000	-1.316376000000	-0.049016000000
C	-2.951673000000	-0.571068000000	-0.674500000000
H	-2.982793000000	-0.260604000000	-1.726918000000
H	-1.226119000000	1.963176000000	-1.717254000000
H	1.062246000000	1.909207000000	-2.578503000000
H	1.922789000000	4.401988000000	-1.067817000000
H	0.920229000000	3.685067000000	0.918754000000
H	-2.867691000000	1.766979000000	1.283505000000
H	-3.506221000000	-1.156334000000	1.967027000000
H	-4.829239000000	0.448739000000	-0.301772000000
H	-2.534006000000	-1.584310000000	-0.594726000000

thf-VII

Cu	0.000000000000	0.000000000000	0.000000000000
O	-0.101310000000	1.856577000000	0.012027000000
O	0.096946000000	-1.856503000000	0.023083000000
H	-0.800298000000	-2.228265000000	0.079312000000
H	0.786767000000	2.230776000000	0.143156000000
O	2.118988000000	0.000000000000	0.000000000000
O	-2.115695000000	-0.006147000000	-0.062286000000
C	-2.777309000000	-0.669240000000	-1.198836000000
H	-2.015224000000	-1.223269000000	-1.761467000000
C	-3.858921000000	-1.556313000000	-0.588118000000
H	-3.464750000000	-2.565209000000	-0.396306000000
C	-4.170437000000	-0.848177000000	0.739585000000
H	-4.828305000000	0.017574000000	0.574958000000
C	-2.790518000000	-0.389717000000	1.181408000000
H	-2.781454000000	0.492758000000	1.832692000000
H	-3.192424000000	0.129525000000	-1.829875000000
H	-4.733738000000	-1.645120000000	-1.244469000000
H	-4.639527000000	-1.510674000000	1.478016000000
H	-2.224338000000	-1.205824000000	1.658009000000
C	2.824059000000	0.734417000000	-1.063171000000
C	2.753772000000	0.286540000000	1.291138000000
C	3.848820000000	1.609725000000	-0.349830000000
C	4.134014000000	0.814933000000	0.933698000000

H	2.152981000000	1.043610000000	1.820210000000
H	2.752147000000	-0.649851000000	1.862596000000
H	4.824679000000	-0.016578000000	0.731078000000
H	4.556133000000	1.433691000000	1.735752000000
H	3.412745000000	2.588650000000	-0.102181000000
H	4.744273000000	1.773376000000	-0.962146000000
H	3.294580000000	-0.020116000000	-1.710276000000
H	2.078004000000	1.297804000000	-1.637560000000

thf-VIII

Cu	0.000000000000	0.000000000000	0.000000000000
O	1.895411000000	-0.024230000000	-0.001854000000
O	-1.878693000000	0.185468000000	0.116088000000
O	-0.054909000000	-1.934840000000	-0.126030000000
H	-1.985205000000	1.151844000000	0.177943000000
H	2.196297000000	0.846333000000	-0.315326000000
H	0.901214000000	-2.109024000000	-0.209910000000
O	0.000000000000	2.264749000000	0.000000000000
C	0.755851000000	2.936605000000	1.059521000000
H	1.231512000000	2.161560000000	1.674190000000
C	1.746031000000	3.852102000000	0.346608000000
H	2.676356000000	3.309673000000	0.119661000000
C	0.999020000000	4.196205000000	-0.950842000000
H	0.244171000000	4.974788000000	-0.765769000000
C	0.326057000000	2.872464000000	-1.288917000000
H	-0.610700000000	2.970181000000	-1.852766000000
H	0.037306000000	3.503223000000	1.672042000000
H	1.998716000000	4.735537000000	0.946676000000
H	1.664504000000	4.538817000000	-1.753638000000
H	1.007285000000	2.198168000000	-1.834194000000

thf-IX

Cu	0.000000000000	0.000000000000	0.000000000000
O	-1.835511000000	0.114937000000	0.125772000000
O	0.029100000000	-2.044712000000	-0.010432000000
H	0.691235000000	-2.361383000000	-0.657705000000
H	-0.827965000000	-2.378392000000	-0.343659000000
H	-2.188359000000	-0.687748000000	0.551463000000
C	0.721398000000	2.753984000000	0.855345000000
H	1.359963000000	3.561394000000	0.462879000000
C	-0.517453000000	3.288066000000	1.548808000000
H	-0.288363000000	4.132492000000	2.211016000000
C	-1.417690000000	3.692332000000	0.363438000000
H	-2.481857000000	3.567915000000	0.597365000000
C	-0.979723000000	2.765436000000	-0.784007000000
H	-1.731133000000	2.017135000000	-1.052795000000
C	2.745618000000	0.211243000000	-1.242734000000
H	2.165688000000	-0.212309000000	-2.071979000000
C	4.080483000000	-0.482251000000	-1.000415000000

H	4.899491000000	0.021750000000	-1.527945000000
C	4.229710000000	-0.422687000000	0.528671000000
H	4.930467000000	-1.172120000000	0.916655000000
C	2.809663000000	-0.680787000000	1.001020000000
H	2.559341000000	-0.240716000000	1.973601000000
O	0.193523000000	2.017257000000	-0.299303000000
O	1.979523000000	0.000000000000	0.000000000000
H	1.327788000000	2.054361000000	1.438960000000
H	-0.984376000000	2.491128000000	2.144133000000
H	-1.246952000000	4.742393000000	0.091929000000
H	-0.652235000000	3.317501000000	-1.675609000000
H	2.844379000000	1.297227000000	-1.372874000000
H	4.037713000000	-1.527623000000	-1.337642000000
H	4.564010000000	0.574528000000	0.849058000000
H	2.560368000000	-1.752447000000	0.999005000000

thf-X

Cu	0.000000000000	0.000000000000	0.000000000000
O	0.030361000000	-1.838333000000	-0.114378000000
O	0.026837000000	2.014501000000	0.088819000000
H	-0.896428000000	2.312781000000	0.215638000000
H	0.527829000000	2.375345000000	0.846699000000
H	-0.880493000000	-2.180005000000	-0.057374000000
O	-2.005537000000	0.215553000000	-0.036421000000
O	2.032547000000	0.000000000000	0.000000000000
C	2.788705000000	0.879964000000	-0.913281000000
H	2.076809000000	1.559181000000	-1.395706000000
C	3.820717000000	1.572529000000	-0.035860000000
H	3.400160000000	2.488525000000	0.404099000000
C	4.086342000000	0.524457000000	1.055765000000
H	4.753859000000	-0.264251000000	0.679800000000
C	2.696643000000	-0.034293000000	1.315309000000
H	2.673944000000	-1.076331000000	1.655003000000
H	3.248647000000	0.225525000000	-1.667430000000
H	4.722259000000	1.838030000000	-0.601847000000
H	4.526429000000	0.953859000000	1.964390000000
H	2.123358000000	0.597051000000	2.011318000000
C	-2.748615000000	-0.239964000000	-1.236502000000
C	-2.754749000000	-0.168180000000	1.179954000000
C	-3.873830000000	-1.109567000000	-0.698571000000
C	-4.152233000000	-0.487372000000	0.678320000000
H	-2.263245000000	-1.046503000000	1.622540000000
H	-2.689800000000	0.682769000000	1.867765000000
H	-4.746057000000	0.432285000000	0.576869000000
H	-4.676333000000	-1.171653000000	1.357031000000
H	-3.535746000000	-2.150156000000	-0.587580000000
H	-4.749015000000	-1.093658000000	-1.359687000000
H	-3.114472000000	0.668846000000	-1.733498000000
H	-2.038226000000	-0.763750000000	-1.886052000000

DFT-IV-90.0

Cu	-0.000103000000	0.000145000000	-0.000353000000
O	0.029517000000	-1.967867000000	-0.064547000000
O	-0.029350000000	1.968319000000	0.061377000000
O	1.957449000000	0.019863000000	0.298402000000
O	-1.958135000000	-0.019699000000	-0.295363000000
H	-0.920987000000	2.191194000000	-0.258831000000
H	-2.261464000000	0.821856000000	0.088816000000
H	0.921551000000	-2.191388000000	0.254085000000
H	2.261519000000	-0.822420000000	-0.083594000000

DFT-IV-93.9

Cu	-0.000469000000	-0.000334000000	0.004421000000
O	0.015549000000	-1.950951000000	-0.298791000000
O	0.019124000000	1.937240000000	-0.367421000000
O	1.921158000000	0.084453000000	0.433152000000
O	-1.959025000000	-0.073047000000	0.234510000000
H	-0.897615000000	2.128951000000	-0.634545000000
H	-2.201337000000	0.853722000000	0.410389000000
H	0.956908000000	-2.147211000000	-0.453242000000
H	2.145704000000	-0.832821000000	0.671519000000

DFT-IV-97.8

Cu	-0.001946000000	-0.003534000000	0.002481000000
O	-0.027034000000	-1.935448000000	-0.398267000000
O	0.076363000000	1.906871000000	-0.463748000000
O	1.889397000000	0.136802000000	0.521484000000
O	-1.939897000000	-0.115839000000	0.346169000000
H	-0.844621000000	2.149052000000	-0.669955000000
H	-2.227276000000	0.809729000000	0.444691000000
H	0.913711000000	-2.168805000000	-0.496944000000
H	2.161301000000	-0.778826000000	0.714079000000

DFT-IV-101.7

Cu	0.000397000000	-0.000693000000	0.001225000000
O	-0.068489000000	-1.907699000000	-0.489649000000
O	0.122449000000	1.874984000000	-0.583735000000
O	1.858879000000	0.183217000000	0.629951000000
O	-1.909304000000	-0.153990000000	0.454809000000
H	-0.796199000000	2.146590000000	-0.762332000000
H	-2.229400000000	0.761812000000	0.545951000000
H	0.862280000000	-2.176023000000	-0.595843000000
H	2.159383000000	-0.728198000000	0.799612000000

DFT-IV-105.6

Cu	0.005646000000	0.005146000000	-0.000332000000

O	-0.102485000000	-1.861166000000	-0.626319000000
O	0.149441000000	1.842490000000	-0.717668000000
O	1.832389000000	0.214546000000	0.737893000000
O	-1.862843000000	-0.183226000000	0.605625000000
H	-0.762320000000	2.116023000000	-0.924830000000
H	-2.207697000000	0.723319000000	0.699938000000
H	0.817310000000	-2.168114000000	-0.722144000000
H	2.130556000000	-0.689017000000	0.947828000000

DFT-IV-109.5

Cu	-0.001255000000	-0.002248000000	0.002328000000
O	-0.125482000000	-1.849657000000	-0.709599000000
O	0.184635000000	1.763054000000	-0.877327000000
O	1.764510000000	0.258385000000	0.859648000000
O	-1.839575000000	-0.191645000000	0.725708000000
H	-0.717638000000	2.083062000000	-1.057406000000
H	-2.169265000000	0.712067000000	0.878626000000
H	0.788868000000	-2.142858000000	-0.872865000000
H	2.115199000000	-0.630159000000	1.050879000000

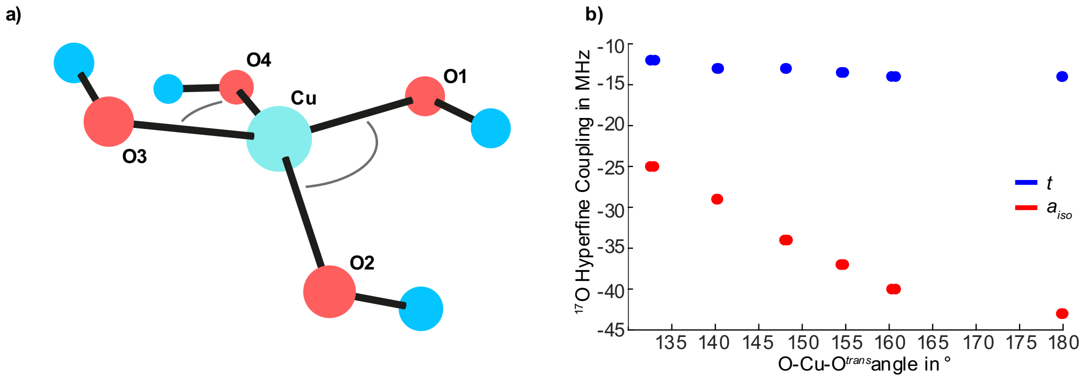

Figure S41. a) Structure of **Cu-IV** after application of O1-Cu-O2 = O3-Cu-O4 angles of 97.8° (**Cu-IV-97.8**), together with **b**) the resulting dependence of t and a_{iso} on the O-Cu-O^{trans} angle (O1-Cu-O3 and O2-Cu-O4).

Table S17. Calculated ^{17}O hyperfine couplings of **Cu-IV** after application of various O1-Cu-O2 and O3-Cu-O4 angles, showing the influence of a geometry distortion on the EPR parameters. The other two O-Cu-O angles were freely optimized. The four OH^- ligands exhibit fairly similar ^{17}O couplings. Hence, only one coupling is listed for ease of reading.

	Constrained O-Cu-O angles	O-Cu-O^{trans} angles	**A** = [A_1, A_2, A_3] in MHz	a_{iso} in MHz	t in MHz
Cu-IV-90.0	90.0°	179.891 179.927	~ [-27, -73, -28]	~ -43 / -44	~ 14
Cu-IV-93.9	93.9°	160.735 160.274	~ [-24, -67, -25]	~ -40	~ 14
Cu-IV-97.8	97.8°	154.529 154.639	~ [-21, -64, -22]	~ -37	~ 14
Cu-IV-101.7	101.7°	148.246 148.057	~ [-19, -60, -19]	~ -34	~ 13
Cu-IV-105.6	105.6°	140.203 140.234	~ [-14, -55, -15]	~ -29	~ 13
Cu-IV-109.5	109.5°	132.561 132.904	~ [-9, -49, -11]	~ -25	~ 12

References

(1) Atherton, N. M.; Horsewill, A. J. Proton ENDOR of $Cu(H_2O)_6^{2+}$ in $Mg(NH_4)_2(SO_2)_4{\cdot}6H_2O$. *Mol. Phys.* **1979**, *37* (5), 1349–1361. DOI: 10.1080/00268977900100991.

(2) Kim, D.; Kim, N. H.; Kim, S. H. 34 GHz Pulsed ENDOR Characterization of the Copper Coordination of an Amyloid β Peptide Relevant to Alzheimer's Disease. *Angew. Chem., Int. Ed.* **2013**, *52* (4), 1139–1142. DOI: 10.1002/anie.201208108.

(3) Burns, C. S.; Aronoff-Spencer, E.; Dunham, C. M.; Lario, P.; Avdievich, N. I.; Antholine, W. E.; Olmstead, M. M.; Vrielink, A.; Gerfen, G. J.; Peisach, J.; Scott, W. G.; Millhauser, G. L. Molecular Features of the Copper Binding Sites in the Octarepeat Domain of the Prion Protein. *Biochemistry* **2002**, *41* (12), 3991–4001. DOI: 10.1021/bi011922x.

(4) Pöppl, A.; Kevan, L. A Practical Strategy for Determination of Proton Hyperfine Interaction Parameters in Paramagnetic Transition Metal Ion Complexes by Two-Dimensional HYSCORE Electron Spin Resonance Spectroscopy in Disordered Systems. *J. Phys. Chem.* **1996**, *100* (9), 3387–3394. DOI: 10.1021/jp9525999.

(5) Jodts, R. J.; Ross, M. O.; Koo, C. W.; Doan, P. E.; Rosenzweig, A. C.; Hoffman, B. M. Coordination of the Copper Centers in Particulate Methane Monooxygenase: Comparison between Methanotrophs and Characterization of the Cu_C Site by EPR and ENDOR Spectroscopies. *J. Am. Chem. Soc.* **2021**, *143* (37), 15358–15368. DOI: 10.1021/jacs.1c07018.

(6) Haak, J.; Golten, O.; Sørlie, M.; Eijsink, V.; Cutsail III, G. pH-Mediated Manipulation of the Histidine Brace in LPMOs and Generation of a Tri-Anionic Variant, Investigated by EPR, ENDOR, ESEEM and HYSCORE Spectroscopy. *ChemRxiv* **2024**, DOI: 10.26434/chemrxiv-2024-jsfbr

(7) Owen, M. E.; Carter, E.; Hutchings, G. J.; Ward, B. D.; Murphy, D. M. Influence of Counterions on the Structure of Bis(Oxazoline)Copper(II) Complexes; an EPR and ENDOR Investigation. *Dalton Trans.* **2012**, *41* (36), 11085–11092. DOI: 10.1039/c2dt31273e.

(8) Bruzzese, P. C.; Salvadori, E.; Jäger, S.; Hartmann, M.; Civalleri, B.; Pöppl, A.; Chiesa, M. ^{17}O-EPR Determination of the Structure and Dynamics of Copper Single-Metal Sites in Zeolites. *Nat. Commun.* **2021**, *12* (1). DOI: 10.1038/s41467-021-24935-7.

(9) Bruzzese, P. C.; Salvadori, E.; Civalleri, B.; Jäger, S.; Hartmann, M.; Pöppl, A.; Chiesa, M. The Structure of Monomeric Hydroxo-Cu^{II} Species in Cu-CHA. A Quantitative Assessment. *J. Am. Chem. Soc.* **2022**, *144* (29), 13079–13083. DOI: 10.1021/jacs.2c06037.

(10) Ross, M. O.; MacMillan, F.; Wang, J.; Nisthal, A.; Lawton, T. J.; Olafson, B. D.; Mayo, S. L.; Rosenzweig, A. C.; Hoffman, B. M. Particulate Methane Monooxygenase Contains Only Mononuclear Copper Centers. *Science* **2019**, *364* (6440), 566–570. DOI: 10.2210/pdb3rgb/pdb.

(11) Cox, N.; Lubitz, W.; Savitsky, A. W-Band ELDOR-Detected NMR (EDNMR) Spectroscopy as a Versatile Technique for the Characterisation of Transition Metal-Ligand Interactions. *Mol. Phys.* **2013**, *111* (18–19), 2788–2808. DOI: 10.1080/00268976.2013.830783.

(12) Colaneri, M. J.; Vitali, J. Probing Axial Water Bound to Copper in Tutton Salt Using Single ^{17}O-ESEEM Spectroscopy. *J. Phys. Chem. A* **2018**, *122*, 6214–6224. DOI: 10.1021/acs.jpca.8b04075.

(13) Silver, B. L.; Getz, D.; Luz, Z. ^{17}O Superhyperfine Interaction in the ESR Spectrum of Hydrated Cu^{2+} Ion. *Chem. Phys. Lett.* **1972**, *13* (2), 113–114. DOI: 10.1016/s0009-2614(72)90001-2.

(14) Getz, D.; Silver, B. L. ESR of $Cu^{2+}(H_2O)_6$. I. The Oxygen-17 Superhyperfine Tensors in $^{63}Cu^{2+}$ Doped Zinc Tutton's Salt at 20°K. *J. Chem. Phys.* **1974**, *61* (2), 630–637. DOI: 10.1063/1.1681939.

(15) Actis, A.; Salvadori, E.; Chiesa, M. Framework Coordination of Single-Ion Cu^{2+} Sites in Hydrated ^{17}O-ZSM-5 Zeolite. *Catal. Sci. Technol.* **2021**, *11* (15), 5191–5199. DOI: 10.1039/d1cy00838b.

(16) Lorenz, A. R.; Ammeter, J. H.; Günthard, H. H. ^{17}O Hyperfine Structure in Single Crystal ESR Spectra of Cu(II) Picolinate:Zn(II) Picolinate·4H_2O. *Chem. Phys. Lett.* **1973**, *23* (4), 463–466.

(17) Lorenz, A. R.; Ammeter, J.; Günthard, H. H. ^{17}O Hyperfine Structure in ESR Spectra of Cu(II) Hydroxyquinolinate: Phthalimide. *Chem. Phys. Lett.* **1972**, *16* (2), 275–277.